

A watershed scale spatially-distributed model for streambank erosion rate driven by channel curvature

Mitchell McMillan*, Zhiyong Hu

*The University of West Florida, Department of Earth and Environmental Sciences,
Pensacola, FL*

Abstract

Streambank erosion is a major source of fluvial sediment, but few large-scale, spatially distributed models exist to quantify streambank erosion rates. We introduce a spatially distributed model for streambank erosion applicable to sinuous, single-thread channels. We argue that such a model can adequately characterize streambank erosion rates, measured at the outsides of bends over a 2 yr time period, throughout a large region. The model is based on the widely-used excess-velocity equation and is comprised of three components: a physics-based hydrodynamic model, a large-scale 1-dimensional model of average monthly discharge, and an empirical bank erodibility parameterization. The hydrodynamic submodel requires inputs of channel centerline, slope, width, depth, friction factor, and a scour factor A ; the large-scale watershed submodel utilizes watershed-averaged monthly outputs of the Noah-2.8 land surface model; bank erodibility is based on tree cover and bank height as proxies for root density. The model was calibrated with erosion rates mea-

*Corresponding author

Email addresses: mcmillan@students.uwf.edu (Mitchell McMillan), zhu@uwf.edu (Zhiyong Hu)

sured in sand-bed streams throughout the northern Gulf of Mexico coastal plain. The calibrated model outperforms a purely empirical model, as well as a model based only on excess velocity, illustrating the utility of combining a physics-based hydrodynamic model with an empirical bank erodibility relationship. The model could be improved by incorporating spatial variability in channel roughness and the hydrodynamic scour factor, which are here assumed constant. A reach-scale application of the model is illustrated on \sim 1 km of a medium-sized, mixed forest-pasture stream, where the model identifies streambank erosion hotspots on forested and non-forested bends.

Keywords: Geographic Information Systems; Root distribution; Meandering streams; Hydraulic modelling

1. Introduction

Streambank erosion is one of the most visible ways that rivers adjust to changes in discharge, sediment supply, and floodplain composition (Leopold and Wolman, 1960). Outer bank erosion, along with inner bank accretion, is responsible for meander migration and the long-term evolution of river channel planforms (Crosato, 2009; Parker et al., 2011; Eke et al., 2014). Not only a key physical process, bank erosion creates and maintains diverse riparian habitats, supplies river channels with large woody material (Florsheim et al., 2008), and is a major source of fluvial sediment (Bull, 1997; Sekely et al., 2002; Kronvang et al., 2013). Over the last few decades, it has become clear that accelerated bank erosion is often a signature of human impacts such as channelization (Hupp and Simon, 1991), agriculture (Knox, 2006; Walter and Merritts, 2008; Kemp et al., 2016), and the pervasive construction and

¹⁴ demise of milldams (Pizzuto and O’Neal, 2009; Merritts et al., 2011; Lyons
¹⁵ et al., 2015). In the U.S., streambank erosion is a major nonpoint source
¹⁶ of sediment pollution (U.S. Environmental Protection Agency, 2000). As
¹⁷ fluvial systems adjust to increasing human influences (Gregory, 2006), it is
¹⁸ important to understand how rates of streambank erosion may respond to
¹⁹ changes in land use/land cover, runoff, and other climate variables (Pelletier
²⁰ et al., 2015).

²¹ Previous studies have investigated the processes that control rates of bank
²² erosion, including weathering, fluvial erosion, and mass wasting. In sinuous
²³ channels, flow around meander bends results in the development of a helical
²⁴ secondary flow, directed inward near the channel bed (Leopold and Wolman,
²⁵ 1960), that produces characteristic bed geometry patterns of shallow point
²⁶ bars and deep pools (Hooke, 1975). The modified bed geometry shifts the
²⁷ primary flow toward the deeper portions of the channel and the outer banks
²⁸ of meander bends (Hooke, 1975; Dietrich et al., 1979; Dietrich and Smith,
²⁹ 1983). These two processes increase the shear stresses acting on the bank,
³⁰ which leads to basal scour and bank steepening. With continued steepen-
³¹ ing, geotechnical instability and eventually bank failure occur (Thorne, 1982;
³² Lawler et al., 1997), possibly followed by slump block armoring (Parker et al.,
³³ 2011). Failure is resisted by effective cohesion, matric suction, and mechani-
³⁴ cal reinforcement by vegetation roots (Osman and Thorne, 1988; Simon et al.,
³⁵ 2000; Pollen and Simon, 2005; Pollen, 2007; Thomas and Pollen-Bankhead,
³⁶ 2010). Although other bank erosion mechanisms dominate in other channel
³⁷ types, this paper is concerned with modelling bank erosion due to channel
³⁸ curvature.

39 Although near-bank shear stress is forced by channel curvature variations,
40 the flow does not instantaneously adapt to these variations; a spatial lag de-
41 velops between maximum curvature and maximum shear stress (Crosato,
42 2009). The spatial lag distance is proportional flow depth and inversely
43 proportional to channel roughness (Blanckaert and de Vriend, 2010), and
44 can be dramatically decreased by vegetation and vegetation-induced bank
45 irregularities (Thorne and Furbish, 1995), further reinforcing the fundamen-
46 tal importance of bank vegetation in the spatial and temporal evolution of
47 streambanks.

48 Floodplain heterogeneity, including the spatial arrangement of vegetation
49 patches, soil characteristics, and land cover types, is an important control on
50 the overall patterns of meandering river channels (Güneralp and Rhoads,
51 2011). Below-ground root distributions remain difficult to quantify, but ob-
52 servations have shown that streambank erosion rates are often sensitive to
53 biomass density (Micheli and Kirchner, 2002; Perucca et al., 2007), root
54 density (Micheli and Kirchner, 2002; Wynn and Mostaghimi, 2006), forest
55 cover (Stott, 1997; Micheli et al., 2004; Allmendinger et al., 2005; Hubble
56 et al., 2010), tree density (Pizzuto and Meckelnburg, 1989; Sass and Keane,
57 2012; Konsoer et al., 2016), and soil properties such as texture and bulk
58 density (Pizzuto, 1984; Couper, 2003; Julian and Torres, 2006; Wynn and
59 Mostaghimi, 2006; Konsoer et al., 2016). On the other hand, recent work
60 on bank erodibility using jet erosion tests suggests that site-specific (rather
61 than watershed-scale) relationships must be derived from soil properties to
62 estimate bank erodibility parameters (Daly et al., 2015). This suggests that
63 while a purely mechanical model of bank failure is likely to require intensive

64 collection of local data, geospatial data such as tree cover may be used as a
65 proxy for some important aspects of bank erodibility such as root reinforce-
66 ment.

67 For cohesive sediments, fluvial erosion is often modeled as proportional to
68 the magnitude of near-bank shear stress above some critical value (Parthe-
69 niades, 1965). Existing models of streambank erosion have quantified near-
70 bank shear stress in a variety of ways. Following the work of Ikeda et al.
71 (1981), a hierarchy of coupled hydrodynamic-morphodynamic models has
72 been developed based on the assumption that bank erosion rate ζ (m/s) is
73 proportional to the excess near-bank velocity,

$$\zeta = E\Delta U \quad (1)$$

74 where ΔU (m/s) is the near-bank excess velocity (near-bank velocity u_b mi-
75 nus reach-averaged velocity U_s), and E is a dimensionless calibration coeffi-
76 cient often called the bank erodibility coefficient (Camporeale et al., 2007).
77 Although it is sometimes assumed that the so-called erodibility coefficient
78 depends only on soil and vegetation properties, it also accounts for numeri-
79 cal constants related to the implementation of a given hydrodynamic model
80 (Mosselman, 2014) as well as any processes of opposite-bank accretion that
81 also drive meander migration (Crosato, 2009; Parker et al., 2011). The ex-
82 cess velocity relationship can be thought of as a linearized form of the excess
83 shear stress equation, and has been tentatively confirmed by field obser-
84 vations (Odgaard, 1987; Odgaard, 1989; Pizzuto and Meckelnburg, 1989)
85 and long-term simulations of natural river reaches (Matsubara and Howard,
86 2014). Equation (1) is an example of a geomorphic transport law (Dietrich
87 et al., 2003).

Models are already available for quantifying soil erosion and transport from drainage basins, but they lack a bank erosion component (de Vente et al., 2013). The applied community (e.g., stream restoration practitioners) employ field-based, empirical models such as Rosgen's BANCS to estimate bank erosion rates (Rosgen, 2001; Simon and Doyle, 2007; Rosgen, 2009), but researchers attempting to calibrate such models have reported mixed results (Harmel et al., 1999; Van Eps et al., 2004; Sass and Keane, 2012; Kwan and Swanson, 2014; McMillan, 2016). Heavy reliance on visual estimates (e.g., of root density), the need for extensive field data collection, and the lack of a process-based near-bank shear stress model diminish the utility of this approach. A recent attempt to extend the BANCS approach with aerial imagery and GIS data demonstrated the need for a spatially distributed bank erosion model, but itself was limited by its empirical, semi-quantitative approach (Bandyopadhyay et al., 2014). While it is impractical to directly simulate all of the processes responsible for erosion at every streambank, a combination of physics-based modelling with empirical calibration can yield powerful predictive tools (e.g., Pelletier, 2012).

In this paper, we test the hypothesis that a curvature-driven model of bank erosion, parameterized by remotely sensed data, can adequately represent point measurements of bank retreat at the outsides of bends over a large region after calibration by field observations obtained over a 2 yr period. The model of this paper quantifies annual streambank erosion rates by employing three interacting submodels: (1) a large-scale, 1-dimensional flow model of monthly discharge and steady uniform flow (streamflow submodel), (2) a physics-based hydrodynamic flow model (hydrodynamic submodel), and

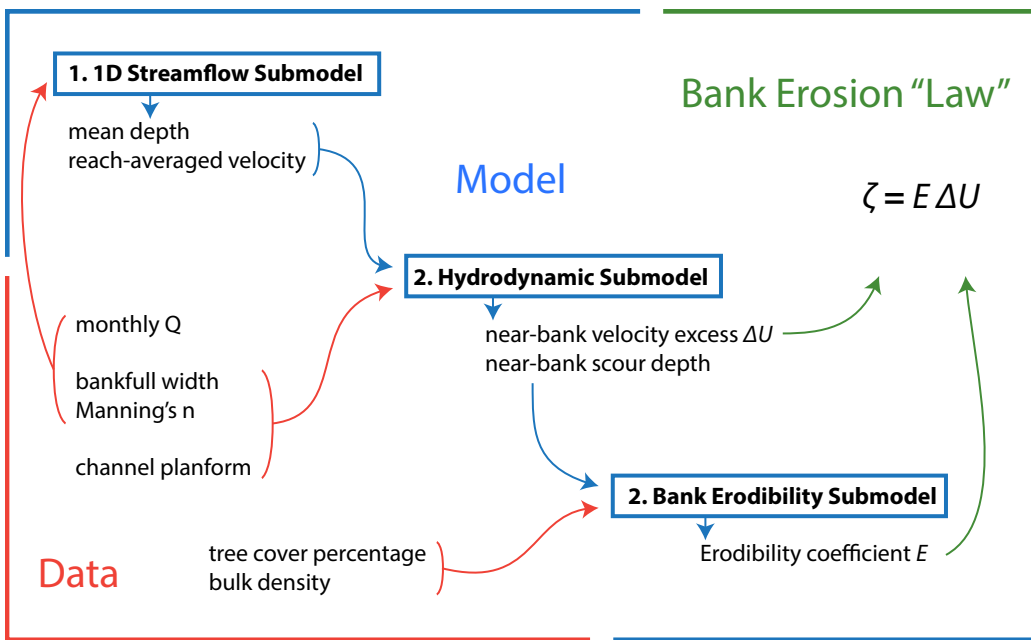


Figure 1: Illustration of model data requirements (red), 3 main components (blue), and the geomorphic transport law used to model streambank erosion rate ζ (green).

113 (3) a model of bank erodibility based on tree cover and bank height (bank
114 erodibility submodel). These submodels, along with their assumptions and
115 limitations are detailed below. Fig. 1 gives a high-level overview of these
116 components, their data requirements, and how they fit into the conceptual
117 model (transport law) for bank erosion.

118 2. Model components

119 Streambank erosion rate $\hat{\zeta}$ (m/yr) was modeled as

$$\hat{\zeta} = E\overline{\Delta U} \quad (2)$$

120 where $\overline{\Delta U}$ (m/s) is the average near-bank velocity excess for a given simula-
121 tion period, and E is bank erodibility (here with units of s/yr). A large-scale
122 1-dimensional model for streamflow was coupled to a hydrodynamic model
123 to estimate ΔU . Two empirical, spatially distributed bank erodibility pa-
124 rameterizations of E were investigated. For model calibration, simulation
125 periods ranged from 22 to 24 mo for each location, depending on the dates
126 of erosion rate measurements. Table 1 summarizes the model input data.

127 2.1. Monthly streamflow model

128 Rather than assuming mean annual discharge or bankfull discharge, a
129 large-scale, 1-dimensional model for streamflow was included to account for
130 spatial and temporal variability in runoff. This component was necessitated
131 by the occurrence of sporadic high precipitation events in the study area,
132 which seemed to be correlated to bank erosion events based on our field
133 experience. The goal of the streamflow model is to estimate monthly flow

Model input		Units	Reference	Data source
<i>Monthly time series</i>				
*Streamflow	Q_m	m^3/s	Xia et al. (2012)	NLDAS-2, Noah-2.8 model
*Storm frequency	f_m	-	Rossi et al. (2016)	PRISM
Event discharge	Q^	m^3/s		Q_m/f_m
*Mean flow depth	H	m		Manning's equation
<i>Time-constant</i>				
*Mean depth	H_0	m	Metcalf et al. (2009)	Regional curves
*Width	B	m	Metcalf et al. (2009)	Regional curves
*Friction factor	$C_{f,0}$	-	Arcement and Schneider (1989)	Table 3
*Channel slope	S	m/m		Extracted from DEM
†Curvature	R^{-1}	m^{-1}	Güneralp and Rhoads (2007)	USGS NED 3m
†Tree cover	TC	%	Sexton et al. (2013)	USGS NED 3m
†Bulk density	BD	g/cm^3	USGS Data Series 866	SSURGO
Scour factor	A	-		Assumed const. = 3

*Reach-averaged. †Spatially variable at the reach scale.

NLDAS-2: National Land Data Assimilation Systems (<https://ldas.gsfc.nasa.gov/nldas/>)

PRISM: PRISM Climate Group, Oregon State University (<http://prism.oregonstate.edu>)

USGS NED 3m: National Elevation Dataset, 3 m per pixel (<https://datagateway.nrcs.usda.gov/>)

GLCF: Global Land Cover Facility, The University of Maryland (www.landcover.org).

SSURGO: Soil Survey Geographic Database (USDA). (<https://dx.doi.org/10.3133/ds866>)

Table 1: Sources of data inputs for the streambank erosion model.

¹³⁴ depth H_m and reach-average velocity U for input into the hydrodynamic
¹³⁵ model. For H_m , Manning's equation can be written in terms of discharge as

$$Q = \frac{1}{n} \frac{A_c^{5/3}}{P^{2/3}} S^{1/2} \quad (3)$$

¹³⁶ where Q is water discharge (m^3/s) A_c is cross-sectional area (m^2), P is wetted
¹³⁷ perimeter (m), S is longitudinal slope (m/m), and n is Manning's roughness
¹³⁸ coefficient. Assuming a rectangular channel cross-section with flow of mean
¹³⁹ depth H_n and width B , then $A_c = BH_n$ and $P = B + 2H_n$. Substituting
¹⁴⁰ these expressions into Eq. (3) yields

$$Q = \frac{1}{n} \frac{(BH_n)^{5/3}}{(B + 2H_n)^{2/3}} S^{1/2} \quad (4)$$

¹⁴¹ where, under the assumptions of steady uniform flow, H_n (m) is the depth
¹⁴² that corresponds to a given discharge, roughness, width, and slope: the so-
¹⁴³ called normal depth. Equation (4) can be solved for H_n using a variety of
¹⁴⁴ methods (Vatankhah, 2013). Here, Eq. (4) was solved using Newton's method
¹⁴⁵ (Tiwari et al., 2012). Monthly discharge was provided by the Noah-2.8 land
¹⁴⁶ surface model described below (Sexton et al., 2013). For each month, reach
¹⁴⁷ average velocity (m/s) was calculated as

$$U = Q*/(BH_n) \quad (5)$$

¹⁴⁸ where $Q*$ represents an estimate of the average monthly discharge during
¹⁴⁹ high flow events. Although the use of a 1-dimensional model is necessarily
¹⁵⁰ simplified, the hydrodynamic model only requires estimates of 1-dimensional
¹⁵¹ flow variables, reach-averaged velocity U and flow depth H_n .

152 2.2. *Hydrodynamic model*

153 The hydrodynamic model component drives streambank erosion by pro-
154 viding the near-bank velocity excess ΔU (Eq. (1)). The hydrodynamic model
155 developed by Blanckaert and de Vriend (2003, 2010) was chosen because, un-
156 like other reduced-order models, it does not assume mild curvature or weak
157 curvature variations (Ottevanger et al., 2012). Because hydrodynamic mod-
158 els built on mild-curvature assumptions can overestimate the effects of sec-
159 ondary flow in sharp bends (Ottevanger et al., 2012), the model of Blanckaert
160 and de Vriend (2010) was considered more appropriate for the study area,
161 where sharp bends are common (Fig. 5). Source code for this model has
162 been provided by Ottevanger et al. (2013) through the OpenEarth reposi-
163 tory (<https://publicwiki.deltares.nl/display/OET/OpenEarth>).

164 In the hydrodynamic model of Blanckaert and de Vriend (2010), hereafter
165 referred to as the BdV model, the downstream velocity width-distribution,
166 which leads to near-bank velocity perturbations, is parameterized by α_s/R ,
167 where $\alpha_s = -1$ corresponds to a potential vortex distribution and $\alpha_s = 1$ to a
168 forced vortex distribution. In straight reaches, α_s is near zero and near-bank
169 velocity is close to the average velocity (Blanckaert and de Vriend, 2003).
170 The streamwise development of α_s/R is represented by a relaxation equa-
171 tion. The relaxation equation has an adaptation length largely controlled by
172 $C_f^{-1}H/R$, and driving mechanisms representing transverse slope, curvature
173 forcing, secondary flow, and velocity redistribution by the secondary flow
174 (Blanckaert and de Vriend, 2010, equations 35–37). Near-bank depth excess
175 Δh (m) is induced by basal scour and is given by $\Delta h = HA/R$, where the
176 A/R term parameterizes transverse bed slope. The streamwise development

¹⁷⁷ of A/R is represented by a relaxation equation with an adaptation length
¹⁷⁸ dependent on H and C_f (Blanckaert and de Vriend, 2010, equation 20).

¹⁷⁹ Natural rivers show variability in the scour factor A , but a typical range
¹⁸⁰ of 2.5 to 6 is often cited (e.g., Ikeda et al., 1981; Ottewanger et al., 2012),
¹⁸¹ or A is treated as a calibration parameter (Odgaard, 1987). In this model,
¹⁸² A was assumed a constant value of 3. Although our field data do not allow
¹⁸³ characterization of A throughout each reach, the average value of A mea-
¹⁸⁴ sured from individual cross-sections was 2.9, which supports our estimated
¹⁸⁵ constant value of 3. Modeled bed topography was initialized before beginning
¹⁸⁶ the simulations by setting $A = 3$ and allowing A/R to adjust to bankfull flow
¹⁸⁷ conditions. A was then kept constant throughout monthly simulations. As-
¹⁸⁸ suming a constant A is a limitation of this implementation, which is designed
¹⁸⁹ to be applicable at the reach and watershed scale by using remotely-sensed
¹⁹⁰ data. If this is not a requirement, spatial variations in A can be measured in
¹⁹¹ the field.

The near-bank values of ΔU (m/s) and Δh (m) were obtained throughout
each reach by the following equations

$$\Delta U = U_s \frac{\alpha_s}{R} \frac{B}{2} \quad (6)$$

$$\Delta h = H \frac{A}{R} \frac{B}{2} \quad (7)$$

¹⁹² where U_s is the reach-averaged velocity (m/s) and H is the cross-sectional
¹⁹³ average flow depth (m) given by the 1-dimensional streamflow model (Sec-
¹⁹⁴ tion 2.1). Bank height was modeled as the bankfull mean depth plus the
¹⁹⁵ near-bank depth excess due to basal scour, $H_b = H_0 + \Delta h$. This height
¹⁹⁶ corresponds to the underwater portion of the bank in the BdV model and

197 does not account for floodplain elevation. Natural streams are thus likely
198 to have higher banks than H_b predicts. A more accurate estimate of bank
199 height could be made by adding H_b to bank heights extracted from a high
200 resolution digital elevation model, which would represent the subaerial por-
201 tion of the banks. The data currently available do not permit this for the
202 studied reaches. As a consequence, the bank heights of most studied reaches
203 are under-predicted by the current model.

204 The BdV model assumes a linear transverse velocity profile that is equal
205 to the reach-averaged velocity at the channel centerline. Therefore, only one
206 bank has a positive velocity perturbation ΔU , while the opposite bank has
207 an equally strong negative velocity perturbation. Meander migration models
208 based on Eq. (1) have usually assumed that channel width remains constant
209 over the simulation period (Parker et al., 2011), and thus that deposition
210 occurs on the opposite bank to keep pace with the eroding bank. The model
211 of this paper is concerned with monthly to annual erosion rates, and not with
212 long-term channel evolution and meander migration. Therefore, it does not
213 make any assumptions about the accretion of the opposite bank. Instead,
214 ΔU is set to zero at locations where it is modeled to be negative. As a con-
215 sequence of this set of assumptions, erosion is only allowed to occur where
216 $\Delta U > 0$ and it is restricted to only one side of a given cross-section. This
217 is a limitation of many meander morphology models, including the present
218 one. It is worth noting, however, that the eroding bank does not necessarily
219 correspond to the concave bank in this model; due to the BdV model's non-
220 linear parameterization of the flowfield and the spatial lag between curvature
221 and velocity perturbations, the convex bank may host positive ΔU values,

especially in tight bends. The BdV model was run on a monthly timestep by varying the monthly event discharge and flow depth according to the procedure detailed above. Prior to the initial model simulation of each channel, bankfull discharge and flow depth conditions were simulated to set the initial bed geometry, and this geometry was held constant throughout subsequent monthly simulations.

2.3. Bank erodibility parameterization

The bank erodibility coefficient E of Eq. (2) was assumed to be proportional to soil erodibility, here denoted K . Two representations of soil erodibility, K_1 and K_2 , were investigated. Wynn and Mostaghimi (2006) provided an empirical equation for sandy streambank soils in southwestern Virginia expressed as a function of coarse root density and soil bulk density at the bank toe,

$$K_1 = c_0 \exp(c_1 \ln RD - c_2 BD^{2.5}) \quad (8)$$

where RD is root density, defined as the volume of coarse roots (2–20 mm in diameter) per volume of soil (cm^3/cm^3), BD is soil bulk density (g/cm^3), and K_1 is soil erodibility with units of $\text{cm}/\text{N}/\text{s}$ (Wynn and Mostaghimi, 2006). Due to the normalization and empirical fitting of the original data by Wynn and Mostaghimi (2006), we replaced the coefficients with generic calibration constants, c_0 , c_1 , and c_2 ; the exponent of 2.5 was retained. Pizzuto (1984) and Pizzuto and Meckelnburg (1989) found that for forested streambanks, bank erodibility was not related to soil properties but was largely controlled by vegetation density. Therefore, the second representation of soil erodibility

²⁴⁴ was a power function of root density RD ,

$$K_2 = c_3 RD^{c_4}, \quad (9)$$

²⁴⁵ where root density is defined as the total volume of roots per volume of soil
²⁴⁶ (cm^3/cm^3), and c_3 and c_4 are calibration constants. In both K_1 and K_2 ,
²⁴⁷ RD was estimated as a function of tree cover and bank height. Because root
²⁴⁸ distributions decrease exponentially with depth below the ground surface
²⁴⁹ (Zeng, 2001), RD at the bank toe was modeled as a function of tree cover
²⁵⁰ and bank height,

$$RD = c_5 TC^{c_6} \exp(c_7 H_b) \quad (10)$$

²⁵¹ where TC is tree cover (the fraction of ground area covered by vegetation
²⁵² >5m tall), H_b is bank height (m), and c_5 , c_6 , and c_7 are calibration constants.
²⁵³ Equation (10) assumes that all trees are growing on a flat floodplain area
²⁵⁴ adjacent to the bank, and not on the bank itself, and thus underestimates
²⁵⁵ the effects of trees growing directly on the bank. Two model formulas were
²⁵⁶ fitted separately, one assuming $E = K_1$, and another assuming $E = K_2$
²⁵⁷ Table 2. After combining calibration constants as appropriate, these models
²⁵⁸ contain 4 and 3 free parameters, respectively. The following sections detail
²⁵⁹ the implementation of this model and present the results of calibrating the
²⁶⁰ model using streambank erosion rates measured over a period of 2.5 yr in
²⁶¹ the northern Gulf of Mexico coastal plain.

²⁶² 3. Data sources and processing

²⁶³ 3.1. Streambank erosion calibration database

²⁶⁴ Streambank erosion rates were measured during the 2014, 2015, and 2016
²⁶⁵ water-years at 30 streambank locations throughout the northern Gulf of Mex-

Model formula	Bank erodibility	Free parameters*
$\hat{\zeta}_1 = a_0 \exp(a_1 \ln(TC) + a_2 H_b + a_3 BD^{2.5}) \overline{\Delta U}$	K_1 (Eq. (8))	a_0, a_1, a_2, a_3
$\hat{\zeta}_2 = b_0 TC^{b_1} \exp(b_2 H_b) \overline{\Delta U}$	K_2 (Eq. (9))	b_0, b_1, b_2

* $a_0 = c_0 \exp(c_1 \ln c_5)$, $a_1 = c_1 c_6$, $a_2 = c_1 c_7$, $a_3 = c_2$
* $b_0 = c_0 c_3 c_5$, $b_1 = c_3 c_4$, $b_2 = c_7 c_4$

Table 2: Two model formulas fitted in this paper. The models differ by their parameterization of soil erodibility and number of free parameters. $\hat{\zeta}$: Modeled streambank erosion rate (m/yr). TC : Tree cover fraction. H_b : Modeled bank height (m). BD : Soil bulk density (g/cm³). $\overline{\Delta U}$: Average near-bank velocity excess (m/s).

266 ico coastal plain (Fig. 2). The study locations were selected to represent
267 variability in channel size, geometry, and vegetation density. All channels
268 included in this study are single-thread, meandering, sand-bed channels, the
269 dominant channel type in the study area (Metcalf et al., 2009). A majority
270 of studied channels (20) were Rosgen type E, which corresponds to sinuous
271 channels with low width-to-depth ratios generally <12 (Rosgen, 1994). Ros-
272 gen type C streams were also common (7 sites), while type F (2 sites) and
273 type G (1 site) streams, which correspond to incised channels, were relatively
274 rare. Metcalf et al. (2009) also identified predominately type C and E streams
275 in the study area. Only wadeable streams were studied. Drainage areas were
276 relatively small, most being <100 km². Streambank characteristics measured
277 in the field are summarized in Fig. 3.

278 Streambank erosion was monitored using repeated cross-profiling, which
279 involved measuring the distance to the bank from a rebar pin placed at the
280 bank toe (Lawler, 1993). Measurements were taken at vertical intervals of

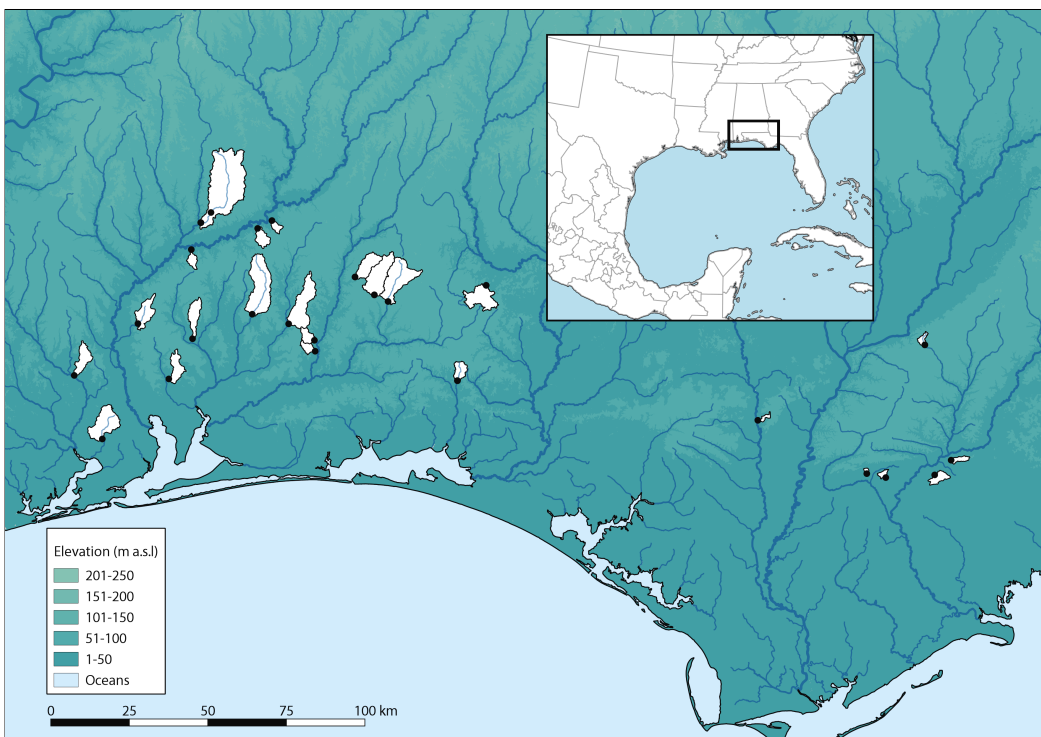


Figure 2: Elevation map showing locations of measured streambank erosion rates (black circles) and their corresponding watershed areas (white). Inset map: Location of the study area within the northern Gulf of Mexico coastal plain.

281 5–50 cm, depending on bank height, and at major breaks in slope (Bangen
282 et al., 2014). Vertical profiles were measured once per year, resulting in
283 final streambank erosion rates averaged over approximately two years for
284 each location. In addition to the vertical profile sections, full channel cross-
285 sections were measured during the initial and final site visits, and were used
286 to determine channel geometry.

287 Erosion rates ranged from 0–1.38 m/yr and were heavily right-skewed,
288 with a mean of 0.094 m/yr, median of 0.027 m/yr, and standard deviation
289 of 0.26 m/yr (Fig. 4). A majority of the studied streambanks (21) had
290 low erosion rates, <0.05 m/yr, including three with no measurable erosion
291 or slight deposition. Because this paper models erosion processes and not
292 deposition, locations that had negative erosion rates ($n = 4$) were assigned
293 values of zero and included in the modelling. Two streambanks retreated at
294 rates greater than 0.4 m/yr; these outliers are apparent in the histogram in
295 Fig. 4 and even on the log-transformed data in Fig. 3. Erosion rates were
296 thus low on average but highly variable.

297 Because the model was designed to utilize widely available remote sensing
298 data, rather than field data collection, no other field measurements were
299 incorporated into model. Bankfull channel widths and depths measured at
300 single cross-sections are included in Fig. 3 for comparison to the modeled
301 values of width and depth obtained through regional curves as described
302 below.

303 *3.2. Channel geometry data*

304 Bankfull channel width B (m) and bankfull mean depth H_0 (m) were
305 estimated using regional curves developed by Metcalf et al. (2009). Regional

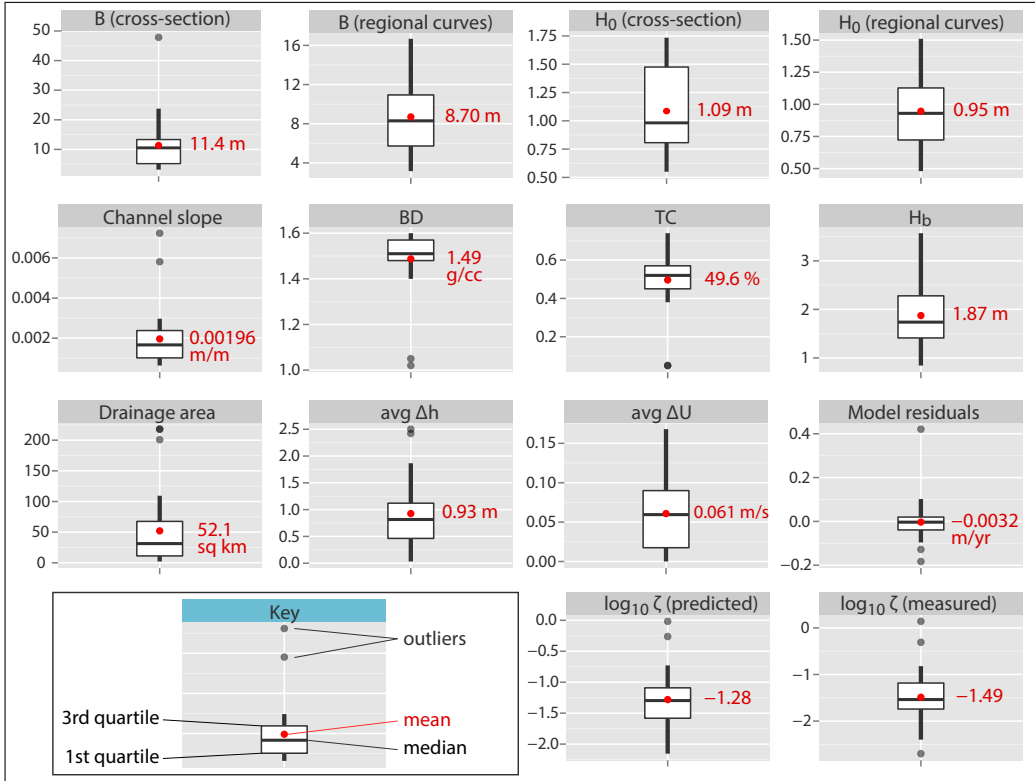


Figure 3: Box-and-whisker plots of field measured data, model inputs, model predictions, and residuals. The whiskers extend to the largest (or smallest) observations that are within 1.5 times the interquartile range of the boxes. Outliers are data points that lie outside of the range of the whiskers. Average values refer to the average of the monthly time series at each study site. Erosion rate statistics do not include values less than or equal to zero.

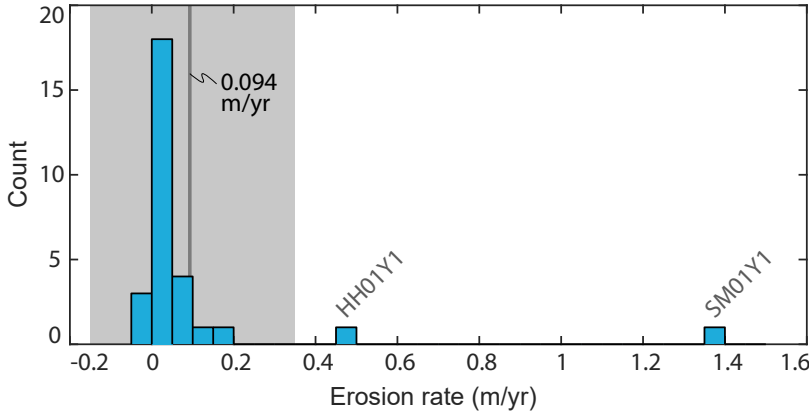


Figure 4: Histogram of measured erosion rates, averaged over 2 yr, including those less than or equal to zero. Bin widths are equal to 0.05 m/yr. The mean (0.094 m/yr) is shown as the thick gray line. The shaded area represents 1 standard deviation (0.26 m/yr) on either side of the mean. Two outliers are labeled with identifiers that correspond to their rows in the supplementary data table.

306 curves predict bankfull channel geometry from drainage area. Similar equa-
 307 tions are available in many regions of the United States (Faustini et al., 2009;
 308 Bieger et al., 2015). In the U.S., the Natural Resources Conservation Service
 309 maintains a database of regional curve studies organized by physiographic
 310 province (NRCS, Regional Hydraulic Geometry Curves, http://www.nrcs.usda.gov/wps/portal/nrcs/detail/national/water/?cid=nrcs143_015052). If
 311 regional curves are unavailable, channel geometry can be estimated with
 312 other methods or measured in the field. For a given reach, B was held con-
 313 stant throughout all model simulations and H_0 was only used to set the initial
 314 bed geometry. Spatial and temporal variation in flow depth were modeled
 315 explicitly (Section 2.2).

317 Drainage areas were extracted from the National Hydrography Dataset
 318 (NHD) Plus v2 using the NHD Plus v2 Basin Delineator Tool. Due to heavy

319 tree cover, channel centerlines were digitized on USGS 3D Elevation Pro-
320 gram (3DEP) DEM (horizontal resolution 1–3 m. In less heavily-forested
321 areas, channel centerlines can be accurately digitized using aerial or satellite
322 imagery (Güneralp and Rhoads, 2007; Güneralp et al., 2013; Güneralp et al.,
323 2014).

324 Digitized centerlines were interpolated with parametric piecewise-cubic
325 spline (PCS) functions $X(s)$ and $Y(s)$, where s is downstream distance (m),
326 and curvature was calculated analytically as

$$\frac{1}{R} = \frac{X'Y'' - Y'X''}{[(X')^2 + (Y')^2]^{3/2}} \quad (11)$$

327 where R is radius of curvature (m) (Güneralp and Rhoads, 2007). The down-
328 stream coordinate s , curvature $1/R$, and unit normal vectors n were dis-
329 cretized at intervals of $B/10$ meters. Fig. 5 plots these interpolated channel
330 centerlines, which were ultimately used to train the model. Channel gra-
331 dients were estimated by extracting a topographic profile along the channel
332 centerline and robust weighted linear regression fitting. For four reaches (five
333 individual sites) that were not resolved by the 3DEP DEM due to especially
334 dense vegetation cover, a 50 cm DEM was created from terrestrial laser scan-
335 ning (TLS) data collected during the study period. These reaches included
336 Willacoochee Creek (sites WC01 and WC02; Fig. 6), Blue Creek (site OR01)
337 Grab Mill Creek (site GM01), and Hollis Branch (site CH01). TLS DEMs
338 were obtained data by taking the minimum height of each 50 cm grid cell
339 (Fig. 6).

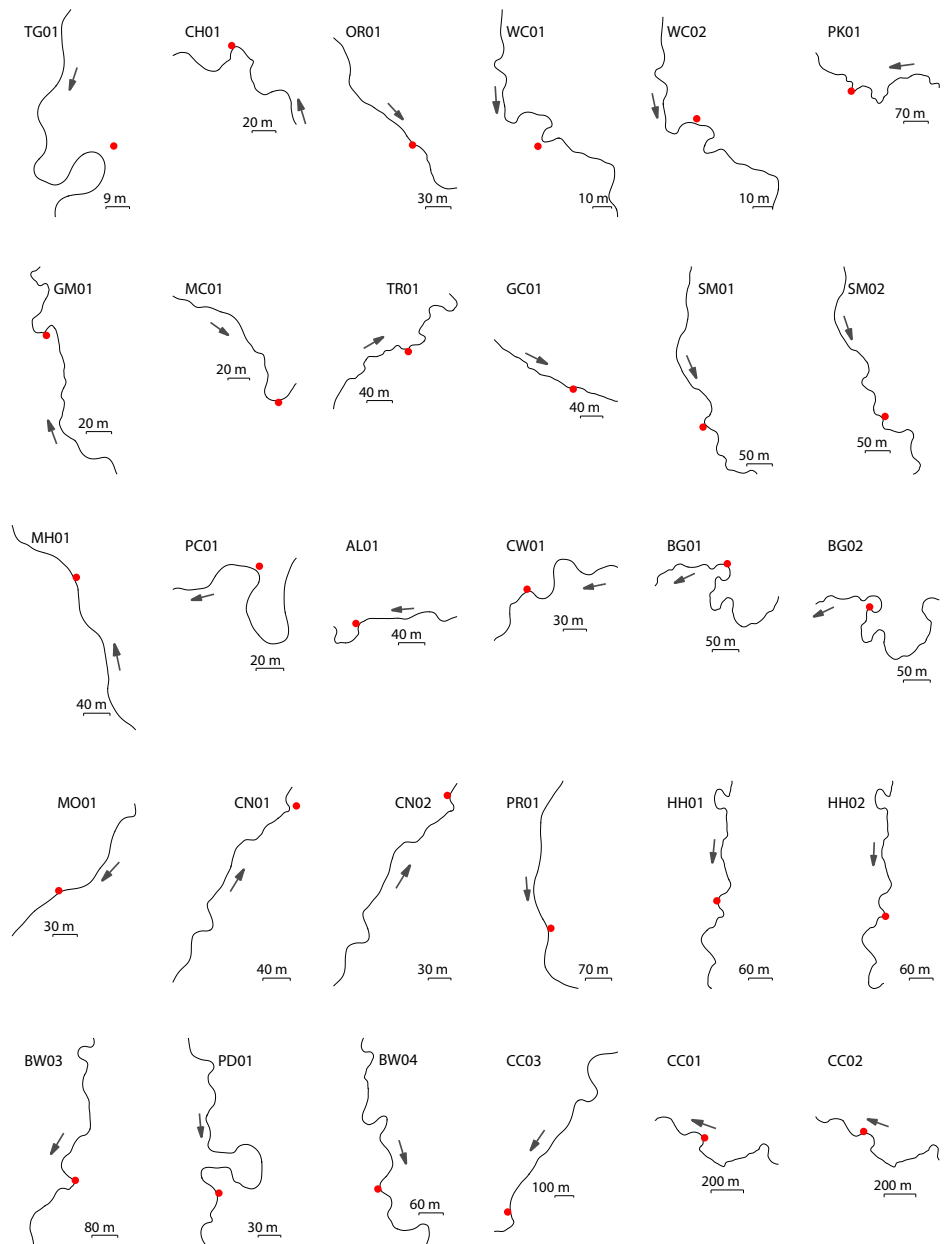


Figure 5: Illustration of channel centerlines derived from piecewise-cubic spline interpolation. Red dots show the locations of streambank erosion monitoring sites. Arrows indicate the general flow direction.

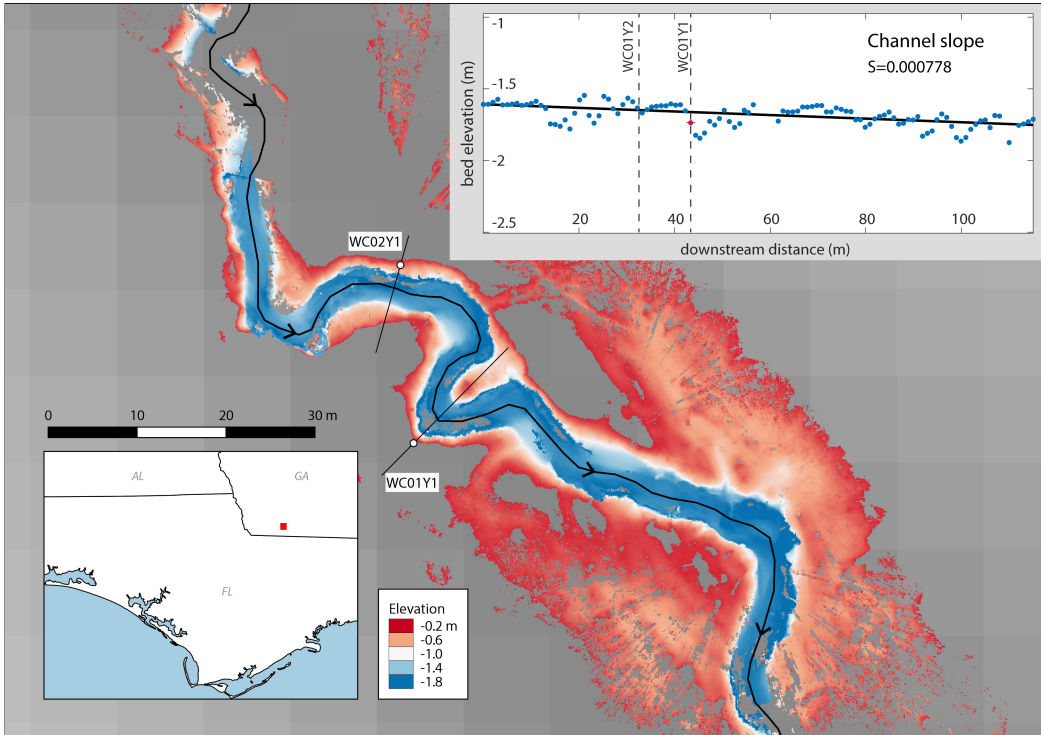


Figure 6: Example DEM created from TLS data collected during the study period overlaid on a DEM of the highest-available resolution at the time of writing (10 m National Elevation Dataset) showing two streambank erosion monitoring sites (WC01, WC02) and the digitized channel centerline (black polyline with arrows indicating flow direction). The upper right inset shows the channel profile extracted from this reach (blue dots), and the robust linear regression line used to estimate channel slope (black line) with 80x vertical exaggeration. Willacoochee Creek, SW Georgia.

340 3.3. *Monthly streamflow data*

341 The Noah-2.8 land surface model (LSM) with National Land Data Assim-
342 ilation Systems Phase 2 (NLDAS-2) forcings (Mitchell et al., 2004; Xia et al.,
343 2012) allowed calculation of the average monthly discharge, Q_m (m^3/s), from
344 each drainage basin. These data are available in $1/8^\circ$ grid cells representing
345 average values within each cell. This scale is similar in size to many of the
346 watersheds in this study. Due to the coarse resolution, a pre-processing step
347 was applied of cubic convolution downscaling to ~ 100 m. Q_m was computed
348 as the sum of basin-accumulated baseflow and surface runoff during each
349 month.

350 Streamflow was simulated for each month by assuming a monthly event
351 discharge, i.e., the average discharge through the channel during periods
352 of high flow events. We assume that this event discharge is more relevant
353 for bank erosion than average monthly or average annual discharge, which
354 tend to be significantly lower due to long periods of baseflow. A simple
355 method was devised to quantify the event discharge Q_m^* for each month m
356 as $Q_m^* = Q_m/f_m$, where Q_m (m/s) is average monthly discharge, and f_m is
357 monthly storm frequency (dimensionless). Average monthly storm frequency
358 was calculated from daily gridded precipitation rasters from the PRISM Cli-
359 mate Group (www.prismclimate.org) as the ratio of wet days (>1 mm
360 precipitation) to total days in each month (Rossi et al., 2016). Note that as
361 storm frequency approaches one, Q_m^* approaches the average monthly dis-
362 charge, and as storm frequency decreases toward zero, Q_m^* increases relative
363 to Q . This reflects the strong effects that large, infrequent storms may have
364 on streamflow. Q_m^* was assigned to zero for months with $f_m = 0$, though

365 this did not occur during the study period.

366 *3.4. Channel friction*

367 Dimensionless channel friction is defined as the square of the shear veloc-
368 ity divided by average velocity,

$$C_f = \left(\frac{u_*}{U_s} \right)^2 \quad (12)$$

369 where $u_* = \sqrt{\tau/\rho}$ is the shear velocity (m/s), τ is average boundary shear
370 stress (Pa), and ρ is the density of water (kg/m^3). The hydrodynamic model
371 described below requires the dimensionless friction factor for a theoretical
372 straight channel, $C_{f,0}$, and the extra drag induced by meandering is simulated
373 by the hydrodynamic model itself. Therefore, Eq. (12) is written in terms of
374 Manning's roughness coefficient n ,

$$C_{f,0} = \frac{gR_h S}{U_s^2} = g \left(\frac{n}{R_h^{1/6}} \right)^2 \quad (13)$$

375 which allows straight channel roughness to be calculated by assuming a con-
376 stant n . The hydrodynamic model assumes a trapezoidal channel cross-
377 section (rectangular in straight reaches), which allows the hydraulic radius
378 R_h to be calculated as $BH_0/(B + 2H_0)$.

379 Sefick et al. (2015) report that n can be estimated using three general
380 approaches: consulting a table relating n to qualitative channel character-
381 istics, comparing studied channels to photographs of channels where n has
382 been measured, or using empirical relationships based on hydraulic variables.
383 The difficulties in empirically estimating n have been well documented, espe-
384 cially for sand bed channels, where the roughness associated with bedforms

385 changes with discharge (Ferguson, 2010). It is also difficult to account for
386 the large roughness elements introduced by dense vegetation using empirical
387 relationships based on grain size and other bed parameters. As an alter-
388 native, semi-quantitative approach, n can be estimated as the sum of five
389 components times a sinuosity factor m ,

$$n = m(n_b + n_1 + n_2 + n_3 + n_4) \quad (14)$$

390 where n_b is a base coefficient for a given boundary material, and m ranges
391 from 1 to 1.3 to account for the increased drag of meandering channels (Arce-
392 ment and Schneider, 1989). Table 3 gives estimates for n_b and n_1 through n_4
393 used in this study. For n_b , a base value representing bed material roughness,
394 we assumed a median grain diameter of 0.2 mm, corresponding to fine sand,
395 based on our qualitative observations of grain size during field work. The
396 other components, which are semi-quantitative, are also estimated based on
397 field experience. This results in a characteristic value of $n = 0.087$ for a
398 straight channel (letting $m = 1$). This value was assumed constant through-
399 out the study area and corresponds to $C_{f,0}$ values around 0.05–0.11, which are
400 significantly larger than the values for rivers reported by (Ottevanger et al.,
401 2012), but representative of the sharp, narrow, highly vegetated channels
402 in the study area (Thorne and Furbish, 1995). Equation (14) assumes that
403 n is constant for all discharges, does not account for bedform drag, and is
404 based on semi-quantitative estimations of vegetation density, surface irregu-
405 larity, and channel obstruction, and thus amounts to an order of magnitude
406 estimate.

Component	Modeled value	Meaning
n_b	0.012	Sand bed with $D_{50} \sim 0.2$ mm
n_1	0.01	Moderate–severe surface irregularity
n_2	0.015	Frequently alternating cross-section
n_3	0.02	Minor obstruction (< 15% channel area)
n_4	0.03	Large amount of vegetation
m	1.0	Sinuosity = 1 (for BdV model)
n	0.087	Manning’s n in this model

Table 3: Values used to calculate Manning’s n for a theoretical straight channel. D_{50} is median grain diameter. BdV: Blanckaert and de Vriend (2010).

407 3.5. Soil erodibility data

408 Soil erodibility was modeled using K_1 (Eq. (8)) and K_2 (Eq. (9)). Area-
 409 and depth-weighted average bulk density was obtained from the SSURGO
 410 dataset in the form of a 10 m raster (Wieczorek, M. E., USGS Data Series 866,
 411 [http://water.usgs.gov/GIS/metadata/usgswrd/XML/ds866_ssurgo_variables.](http://water.usgs.gov/GIS/metadata/usgswrd/XML/ds866_ssurgo_variables.xml)
 412 xml).

413 Root density RD was modeled as a function of tree cover TC and bank
 414 height H_b (Eq. (10)). Tree cover was obtained as a 30 m raster from the
 415 Global Land Cover Facility at the University of Maryland, which represents
 416 the fraction of each 900 m² pixel covered by vegetation greater than 5 m
 417 in height (Sexton et al., 2013). This dataset is based on Landsat observa-
 418 tions, is free to the public, covers the entire globe, and is readily available
 419 online (<http://www.landcover.org/data/landsatTreecover/>). Three datasets
 420 are available based on observations from 2000, 2005, and 2010. Although ero-

421 sion rates were measured during 2014–2016, the 2010 dataset contains many
422 small gaps associated with cloud cover. Therefore, the 2005 dataset was used.
423 Although the 2005 tree cover dataset is approximately 10 yr out of date, it
424 is highly unlikely that any of the small headwater streams investigated in
425 this study have shifted significantly at the 30 m/pixel scale since 2005. The
426 largest erosion rate observed in this study, \sim 1.3 m/yr, corresponds to a total
427 lateral shift of 13 m over 10 yr, assuming that such a high erosion rate is
428 sustained over the 10 yr period. Additionally, no major forest disturbances
429 were observed at any of the study sites, which would be obvious had they
430 occurred during the last 10 yr in the study area. Most studied streambanks
431 hosted trees of varying species and diameters, which qualitatively supports
432 the moderately high values of tree cover exhibited in the 2005 dataset. Most
433 sites hosted trees greater than 30 cm in diameter, which indicates that they
434 have been growing for much longer than 10 yr. One exception is Sconnier's
435 Mill Creek (sites SM01 and SM02), which has recently lost much of its tree
436 cover in a limited area near the bank. Based on our field experience, an esti-
437 mated value of 5% was assigned as input for this location. All other locations
438 used values from the 2005 tree cover dataset. If this model is applied in more
439 dynamic environments in the future, the 2005 tree cover dataset may prove
440 to be inadequate, in which case the 2010 dataset may be used, or tree cover
441 may be estimated using different methods.

442 *3.6. GIS environment*

443 The raster data representing tree cover, bulk density, and monthly stream-
444 flow and the polylines representing channel geometry were managed in a ge-
445 ographic information system (GIS) using Matlab (Fig. 7). The 30 m pixel

446 size of these raster data is relatively coarse compared to the studied channel
447 reaches. Errors can arise if the raster data are sampled at pixels represen-
448 tative of the opposite streambank or corresponding to the mid-channel open
449 water. Therefore, rasters were sampled at bank locations, rather than chan-
450 nel centerlines. Left- and right-bank locations were modeled as one channel
451 width from each centerline using the unit normal vectors n calculated during
452 PCS-interpolation of the channel centerline. To associate measured erosion
453 rates to a modeled bank location and channel centerline node, the GPS lo-
454 cations recorded in the field were matched with the nearest-neighbor bank
455 location (Fig. 7).

456 Rasters were sampled at runtime by looping through the bank point lo-
457 cations and extracting (Matlab function *imread*) and interpolating the four
458 nearest pixels from the raster dataset. This approach has the advantage that
459 rasters of differing resolution and/or spatial references can be used without
460 the need to reproject the entire raster, provided that geotransforms exist
461 between the various spatial reference coordinates. This allows entire river
462 reaches to be modeled efficiently. Bilinear interpolation results in bank erodi-
463 bility estimates that vary smoothly throughout a meander bend, rather than
464 in sharp jumps characteristic of the raw raster pixels. Each bank location,
465 therefore, is assigned unique values of tree cover and bulk density as well as
466 a value of near-bank velocity excess and bank height from the hydrodynamic
467 model.

468 *3.7. Regression analysis*

469 Given the model structure presented above and the model formulas of
470 Table 2, the free parameters must be estimated by minimizing model error.

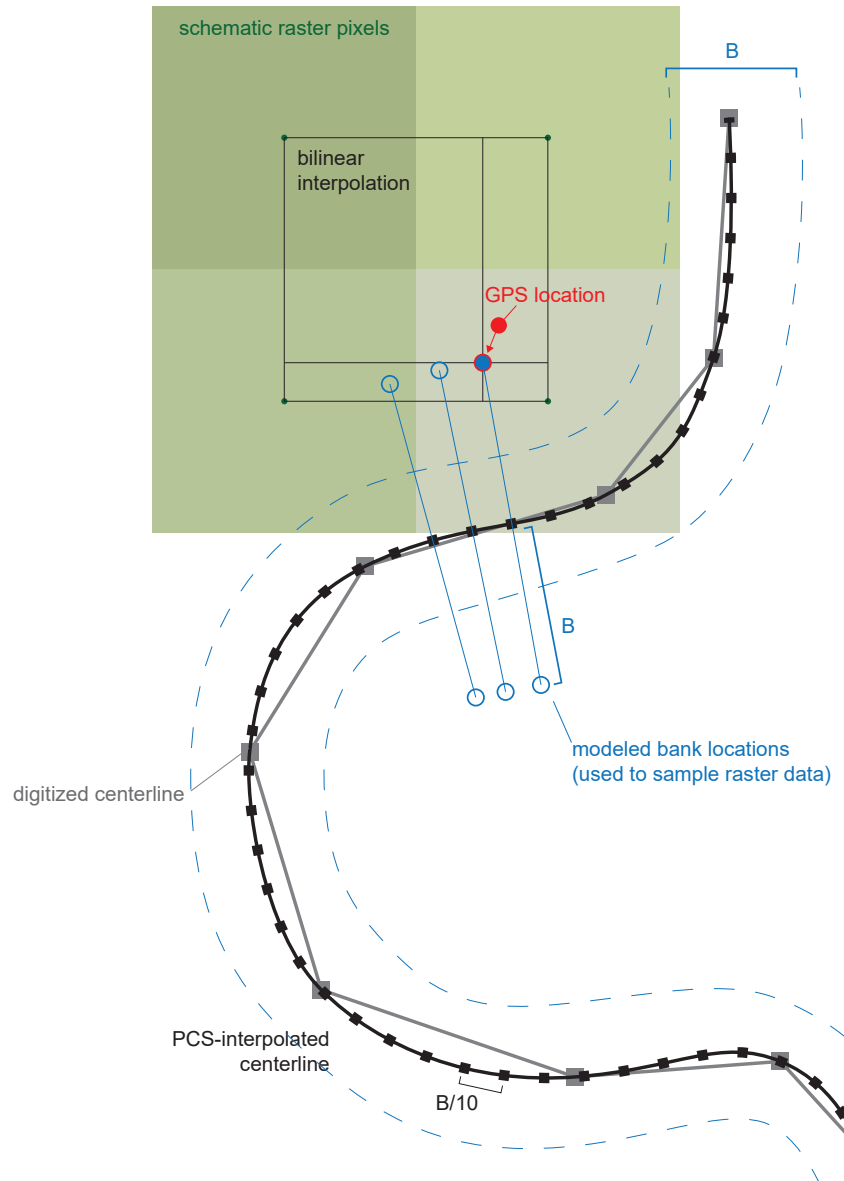


Figure 7: GIS environment. Centerlines digitized on a 3 m DEM (gray polyline) were PCS-interpolated (black). Banks locations (blue circles) were assumed B meters (channel width) from the centerline. The bank point nearest the cross-section as surveyed in the field (red circle) was selected. The 4 nearest raster pixels were interpolated (green squares).

⁴⁷¹ There are at least three straightforward options, however, each with its own
⁴⁷² set of assumptions regarding error structure. Letting $f(x)$ represent an ar-
⁴⁷³bitrary, nonlinear function of independent variables, erosion rate ζ can be
⁴⁷⁴modeled as

$$\zeta = f(x) + \epsilon \quad (15)$$

$$\zeta = f(x) \cdot \epsilon \quad (16)$$

$$\zeta = f(x) \cdot \exp(\epsilon) \quad (17)$$

⁴⁷⁵ where ϵ is normal error, $\epsilon \sim \mathcal{N}(0, \sigma)$. Equation (15) assumes that error
⁴⁷⁶ is additive and normally distributed, Eq. (16) assumes that error is multi-
⁴⁷⁷plicative and normally distributed, and Eq. (17) assumes that error is multi-
⁴⁷⁸plicative and lognormally distributed (Xiao et al., 2011). It is worth noting
⁴⁷⁹that Eq. (17) results from log-transforming both sides of a nonlinear equa-
⁴⁸⁰tion, e.g., a power-law relationship, which is commonly done to linearize the
⁴⁸¹equation for practical or scientific reasons (Xiao et al., 2011). The choice of
⁴⁸²error model can often have a large impact on the final values of regression
⁴⁸³parameters and thus also on the conclusions drawn from modelling studies.

⁴⁸⁴ We investigated all three error models while calibrating the free parame-
⁴⁸⁵ters. Normal additive and normal multiplicative error models were inves-
⁴⁸⁶tigated through nonlinear regression (Matlab function *fitnlm*); lognormal
⁴⁸⁷multiplicative error was investigated by log-transforming the data for the
⁴⁸⁸equations given in Table 2 and linear regression of the log-transformed data.
⁴⁸⁹ Only the normal multiplicative error model (Eq. (16)) resulted in accurate
⁴⁹⁰predictions of streambank erosion rate. Additionally, for stochastic events

491 such as streambank erosion, variance is proportional to the maximum magni-
492 tude of individual events (Pizzuto et al., 2010), which we interpret as further
493 evidence that a regression model with proportional error variance is most
494 appropriate.

495 In the context of nonlinear regression, R^2 is reported as the square of the
496 Pearson correlation coefficient R of the actual and modeled values. However,
497 the streambank erosion rates reported here were not normally distributed
498 (Fig. 4), and two outliers will have a large influence on the regression statis-
499 tics. Because these outliers are due to naturally high erosion rates and not
500 to measurement error, we did not remove them from the dataset, especially
501 because the model is designed to predict streambank erosion hotspots such
502 as these. As a consequence, parametric statistics such as R and R^2 , which
503 are not robust to outliers, are misleading. Therefore, we also report a more
504 robust measure of correlation, Spearman’s rank correlation coefficient, ρ ,
505 which is equal to the Pearson correlation coefficient of the rank values of
506 actual and modeled streambank erosion rates. Although ρ cannot be inter-
507 preted as easily as R or R^2 , it is useful in comparing models from the same
508 dataset.

509 4. Results

510 Two separate models were run using the same input data: one with soil
511 erodibility as K_1 and another with soil erodibility as K_2 . Fig. 9 plots the re-
512 sults of statistical calibration of each model. For $E = K_1$, the fitted equation
513 is given by

$$\hat{\zeta}_1 = 0.0322 \exp [-1.030 \ln(TC) + 0.197H_b + 0.768BD^{2.5}] \overline{\Delta U}. \quad (18)$$

514 Soil erodibility modeled by K_1 was thus predicted to be inversely related to
515 tree cover and directly related to bank height and bulk density. In contrast
516 to this result, Wynn and Mostaghimi (2006) reported a strong inverse rela-
517 tionship to bulk density. Possible reasons for this discrepancy are discussed
518 below.

519 The simpler model incorporating $E = K_2$, in which soil erodibility is a
520 function of bank height and tree cover only, is given by the fitted equation,

$$\hat{\zeta}_2 = 0.294 TC^{-1.05} \exp(0.157 H_b) \overline{\Delta U} \quad (19)$$

521 which suggests that bank erosion rates are directly related to near-bank ve-
522 locity excess and bank height and inversely related to tree cover. According
523 to the root density parameterization (Eq. (10)), the exponent of TC and the
524 coefficient of H_b are expected to be opposite in sign, since root density at the
525 bank toe should increase with tree cover and decrease with bank height. The
526 coefficients and exponents are thus physically sound if streambank erosion is
527 inversely related to root density. Although the data points with measured
528 streambank erosion rates equal to zero ($n = 4$) are not shown on the log-log
529 plots of Fig. 9, they were also predicted by the models. Both models pre-
530 dicted erosion rates of zero for two of the four, i.e., $\overline{\Delta U} < 0$. The model
531 incorporating K_1 predicted the other two to erode at 0.0079 m/yr and 0.047
532 m/yr, a modest overestimate of ~ 1 to 5 cm/yr. The model incorporating K_2
533 predicted negligible values of less than 0.001 m/yr for these two locations.

534 Fig. 8 plots the model's sensitivity on four parameters with significant
535 uncertainty: channel slope S , Manning's n , scour factor A , and monthly dis-
536 charge Q_m . Parameters were varied as percentages of their base values. For
537 n and A , base values were constant for all sites (0.087 and 3 respectively,

described above). For S and Q_m , the base base values are reach-averaged values. Sensitivity analyses for all calibration sites followed similar patterns, illustrated in Fig. 8. The model's response to Manning's n variations, which ranged from 0.0174 to 0.087, showed the most variability. In all cases, as n decreased, high velocity zones progressively shifted onto the inner, rather than the outer banks. We interpret this as a sign that the lowest n values investigated in the sensitivity analysis were not physically realistic for the study reaches. A site's response to changes in n depended on the its location with respect to its meander bend and to adjacent bends. The model's response to variations in monthly Q were similarly variable across sites due to their locations in meander bends. Larger values of Q correspond to lower channel friction (Eq. (13)) and larger flow depths, both of which increase the spatial lag between curvature forcing and velocity perturbations (Blanckaert and de Vriend, 2010). The model's response to variations in S and A was consistent across all study sites, with A having a larger effect on model output (Fig. 8).

This simple sensitivity analysis suggests that the model is most sensitive to changes in Manning's n and to the scour factor A . Future applications of the model could be improved by incorporating spatial variability into these parameters, rather than the constant values we have assumed here.

Fig. 10 shows the results of applying the model with $E = K_2$ to a medium-sized stream in a mixed pasture/forest landscape in Okaloosa County, FL. The simulation was run using the same input data used to train the model, including a monthly discharge time series of 24 mo. A few bends are currently meandering out of the riparian buffer zone into pastured areas, where tree

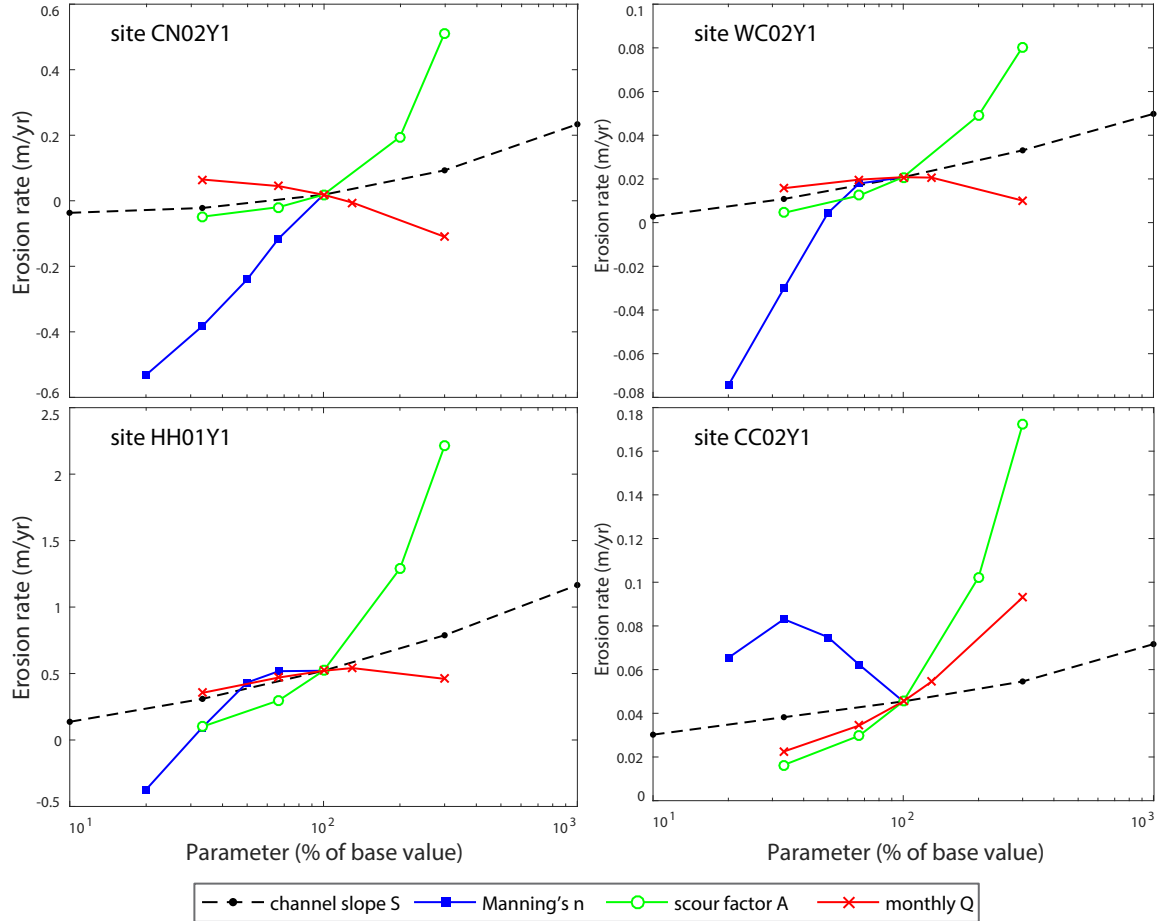


Figure 8: Sensitivity of the modeled streambank erosion rates to 4 model parameters: channel slope S , Manning's n , scour factor A , average discharge Q . Changes in erosion rates resulting from changing each of these parameters independently are plotted for four study sites. The parameters are expressed as percentages of their base values discussed in the text.

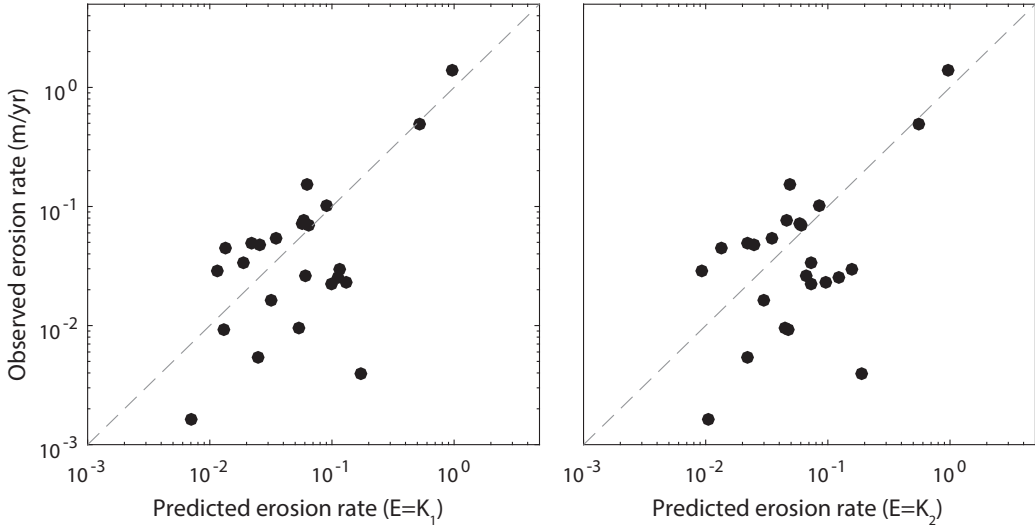


Figure 9: Results of model calibration using soil erodibility parameters K_1 (Eq. (8)) and K_2 (Eq. (9)). The model with K_1 predicts streambank erosion rates with a significant correlation ($R^2 = 0.91, p < 0.001, \rho = 0.53$). The model with K_2 predicts streambank erosion rates to a similar degree ($R^2 = 0.90, p < 0.001, \rho = 0.48$) but with fewer parameters. The dashed line is 1:1 correlation. Here, R^2 represents the square of the Pearson correlation coefficient R between modeled and predicted erosion rates in their original units; ρ is Spearman's rank correlation coefficient. See the text for discussion on interpreting these statistics for this dataset.

563 cover is very low. High erosion rates of >0.75 m/yr were predicted on the
564 non-forested section of the large bend downstream (south) of the calibration
565 locations (HH01 and HH02), and rates of almost 1 m/yr were modeled on
566 a tight, non-forested bend in southern part of the map. The non-forested
567 bends all host erosion rates of well over 0.25 m/yr. Reasonably high erosion
568 rates were not only confined to non-forested bends, however; several sharp
569 bends in the forested portion of the image were predicted to erode up to
570 0.25 m/yr, comparable to the non-forested bend near HH01. The moder-
571 ate erosion rates on these forested bends are associated with increased basal
572 scour resulting from their high curvatures. Additionally, the upstream ge-
573 ometry of the meander train could have a cumulative downstream effect on
574 erosion rates, as shown by Güneralp and Rhoads (2009, 2010). The bottom
575 panel plots channel curvature (B/R), velocity excess ($\Delta U/U$) and depth ex-
576 cess ($\Delta h/H$) against the downstream coordinate s and shows the spatial
577 lag between curvature and the velocity perturbations. Fig. 10 illustrates the
578 model's ability to predict streambank erosion rates throughout a 1 km reach
579 displaying high variability in tree cover and channel geometry characteristics.

580 5. Discussion

581 We presented two models that predicted streambank erosion rates (Fig. 9).
582 While both are highly correlated to observed erosion rates, the model incor-
583 porating K_2 for soil erodibility contains only three free parameters, while the
584 model incorporating K_1 contains four. The negative relationship between
585 bulk density and bank erosion reported by (Wynn and Mostaghimi, 2006)
586 was not observed here. This could be due to many factors. Soils with high

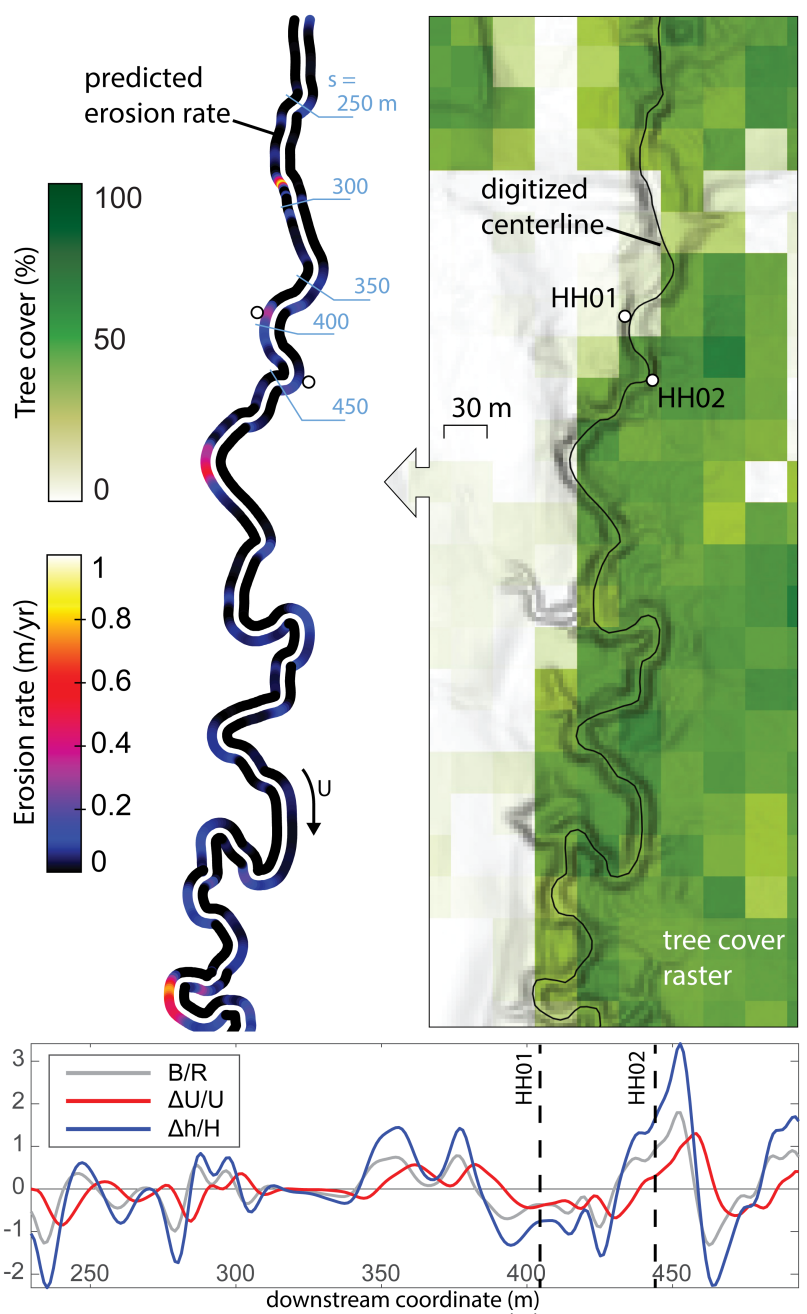


Figure 10: Model application on Horsehead Creek (sites HH01 and HH02). Right: Input tree cover dataset (white to green) and channel centerline digitized on 3 m DEM (shown with slope shaded). Left: Modeled streambank erosion rates throughout the reach. Light blue numbers map the downstream coordinate plotted in the bottom panel. Flow is north to south. Bottom: Comparison of curvature (B/R), velocity excess ($\Delta U/U$), and depth excess ($\Delta h/H$) during the December 2015 simulation.

587 organic matter and root biomass content would express lower bulk densi-
588 ties despite being less erodible overall, and sandy soils commonly express
589 higher bulk densities as well as higher erodibility. The large-scale SSURGO
590 dataset may also be unable to resolve the spatial heterogeneity of bank ma-
591 terials, especially for many of the small channels used to calibrate the model.
592 This result agrees with recent work by Daly et al. (2015), who found that
593 watershed-scale relationships for bank erodibility based on soil properties
594 showed no significant correlations to erodibility coefficient or critical shear
595 stress. It is therefore not surprising that K_1 did not improve the bank erodi-
596 bility estimation across the many watersheds of our study.

597 The overall effectiveness of K_2 agrees with the observations of Pizzuto
598 (1984), Pizzuto and Meckelnburg (1989), and Pizzuto et al. (2010), who found
599 that forested streambank erodibility is largely controlled by tree density. As-
600 suming representative values of tree cover of 5–10% for pastured/agricultural
601 areas and 40–60% for forested areas, Eq. (19) predicts that forested stream-
602 banks retreat 4–12 times slower than non-forested ones. This generally agrees
603 with previous studies, which have reported two to five-fold differences in bank
604 erodibility between forested and non-forested streambanks (Micheli et al.,
605 2004; Allmendinger et al., 2005; Sass and Keane, 2012). The relatively
606 large (up to 12-fold) difference implied here is probably due to the extremely
607 low erosion rates of forested streambanks in these low-gradient coastal plain
608 streams, rather than especially high erosion rates of non-forested stream-
609 banks.

610 In both models, there appear to be two distinct groups of data points, one
611 with largely positive residuals and another with negative residuals. Residuals

were mapped and Moran's Index of $I = -0.09$ was calculated in ArcMap, indicating that the residuals are not spatially autocorrelated and are not statistically different from random ($p = 0.86$). Fig. 11 maps the residuals over Noah-2.8 surface runoff and PRISM precipitation totals for September 2015. Comparison to the PRISM data shows that some highly localized but intense storms were not represented well in the Noah-2.8 runoff simulations, either as a result of the coarse resolution of the NLDAS-2 forcing data, or because of inaccuracies in the Noah-2.8 LSM. Extreme rainfall totals and flash flooding were documented by weather stations in the area during this event (National Weather Service, North Central Gulf Coast Heavy Rain Event 27-29 September 2015, accessed 16 June 2016, https://www.weather.gov/mob/heavyrain_sep2015). It is likely that the Noah-2.8 underestimated surface runoff during such small intense storms, which may have contributed to the negative residuals shown on the map (Fig. 11).

It would be useful to compare the model of this paper to similar models in the literature, but few if any comparable models exist. We therefore fit two simple models for comparison: a purely empirical statistical model and an Ikeda-type model based on Eq. (2) with a spatially constant erodibility coefficient E . All models were fit using the nonlinear regression procedure outlined in Section 3.7. Table 4 shows that the model of this paper, using either K_1 or K_2 , outperforms these simpler models according to Spearman's rank correlation coefficient ρ , which is robust to outliers. R^2 is reported as the square of the correlation coefficient between the predicted and actual streambank erosion rates, but is skewed by outliers. The negative exponents on slope and drainage area exhibited by the purely empirical model are likely

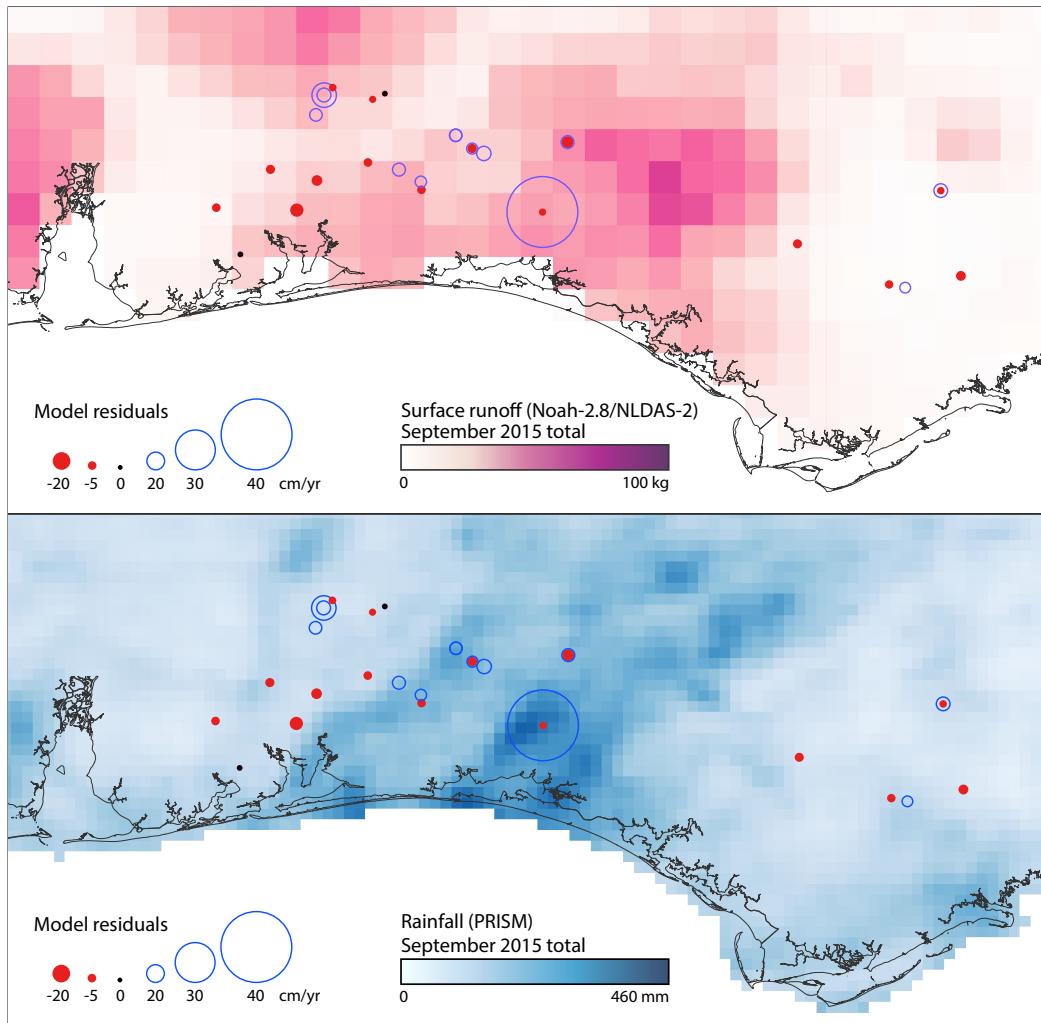


Figure 11: Map of residuals. Comparison of Noah-2.8 surface runoff (top) and PRISM precipitation (bottom) for September 2015 demonstrates discrepancies in the Noah model. A small but intense storm near the middle of the map is not represented in the surface runoff data.

Model	Description	Statistics
Eq. (18)	This paper, K_1	$R^2 = 0.91, \rho = 0.53$
Eq. (19)	This paper, K_2	$R^2 = 0.90, \rho = 0.48$
$\hat{\zeta} = 0.032BD^{-5.4}S^{-0.037}A^{-0.86}TC^{-2.8}$	Empirical model	$R^2 = 0.98, \rho = -0.20$
$\hat{\zeta} = 1.54\overline{\Delta U}$	Eq. (2)	$R^2 = 0.034, \rho = 0.25$

Table 4: Comparison of the model of this paper with a purely empirical model and a model lacking spatial variability in bank erodibility (an Ikeda-type model based on Eq. (1)).

not physically sound, and $\rho < 0$ indicates an overall negative relationship to erosion rates. The Ikeda-type model is positively correlated to erosion rates, but this correlation is not as strong as the models proposed here. This comparison illustrates the utility of combining the BdV hydrodynamic model with a spatially distributed bank erodibility relationship.

An existing spatially distributed model for total sediment yield from drainage basins, SedNet, quantifies annual streambank erosion as a function of bankfull stream power, bank erodibility, and a daily streamflow factor (Wilkinson et al., 2009, 2014). The SedNet model requires a long-term dataset of daily streamflow observations as well as two raster datasets: one representing vegetation cover (values of 0 to 1, with 1 representing fully intact riparian vegetation) and another of bank erodibility (values of 0 or 1, with 0 representing bedrock and 1 representing pixels characterized as soil). Rather than modelling the spatial variability introduced by hydrodynamic processes, SedNet models the average bank erosion of entire stream links. SedNet was not designed to allow the prediction of local streambank erosion rates, or the identification of erosion hot-spots, but rather to simulate the

654 large-scale processes exporting sediment from large drainage basins; stream-
655 bank erosion is just one part of the model. Nevertheless, it is increasingly
656 being used to estimate local streambank erosion rates because it is the only
657 spatially distributed model that attempts to do so (Bartley et al., 2008). One
658 recent evaluation of the accuracy of the streambank erosion rates predicted
659 by SedNet showed that its original predictions differed from measured ero-
660 sion rates (averaged over 10 locations) by a factor of 74, but this discrepancy
661 was decreased to a factor of ~ 2 with calibration to field-measured values of
662 bed slope and bankfull discharge.

663 The main goal of this paper was to develop a spatially distributed model
664 that incorporated widely available data and could be readily used in practical
665 applications. This approach necessitated a few simplifications. Meander
666 migration models based on Equation (1) usually assume some a constant
667 discharge to determine ΔU , e.g., mean annual Q , bankfull Q , or another
668 statistic (Camporeale and Ridolfi, 2010). Here, we computed a monthly-
669 varying discharge statistic Q^* , and ran the BdV model on this timestep
670 before averaging the monthly estimates of ΔU . This approach was designed
671 to account for variability in precipitation and runoff at the regional scale, and
672 for increased erosion during high flow periods. This is a novel application of
673 Eq. (1), however, and it has not been shown that streambank erosion rates
674 are proportional to ΔU on these shorter timescales.

675 The sensitivity analysis showed that the model is sensitive to errors in
676 Manning's roughness coefficient n and the scour factor A , but these parame-
677 ters are difficult to estimate using only remotely sensed data, or other widely
678 available datasets. We assumed characteristic values for these parameters

and held them constant throughout the study area. This is a major limitation of the model and likely a source of error. In the future, reach-scale measurements of n and A should be incorporated into the model.

Another limitation of the model is its reliance on an *ad hoc* method for determining the relevant monthly discharge, which was estimated as a function of average monthly discharge and storm frequency. The lack of streamgages in the basins being studied necessitated modelling of monthly streamflow. The average monthly streamflow estimates are from the Noah-2.8 LSM, a large-scale land surface model designed to simulate processes acting at the global, continental, and large watershed scale. Such models have been shown to be relatively inaccurate at predicting streamflow in small basins, though they often express a higher skill in the southeastern U.S. than in other regions (Xia et al., 2012).

A thorough validation of this model is outside the scope of this paper, but should be done at the reach and watershed scales. The model could be evaluated on a few reaches where channel geometry is known or can be easily measured. Existing streambank erosion rate databases could be useful for model validation, provided that the GPS coordinates of streambank measurements can be determined accurately.

6. Conclusions

Bartley et al. (2008) remarked that “it will be difficult for catchment scale sediment budget models to ever accurately predict the location and rate of bank erosion due to the variation in bank erosion rates in both space and time.” de Vente et al. (2013) cited the lack of a bank erosion component as

703 a major limitation of current sediment detachment models. We presented a
704 spatially distributed model for streambank erosion incorporating an empir-
705 ical soil erodibility parameter (K_2), a nonlinear hydrodynamic model, and
706 monthly discharge forcings. An application of the model to a medium-sized
707 stream in the Gulf Coastal plain (Fig. 10) demonstrated its potential for
708 quantifying annual streambank erosion throughout a mixed forest/pasture
709 reach. Although future work should focus on improving the model's param-
710 eterization of roughness and streamflow, as well as a thorough evaluation
711 and validation of model predictions throughout multiple reaches, the current
712 model shows a significant correlation to observed erosion rates. The model
713 thus represents a first step toward filling the long-standing gap emphasized
714 by Bartley et al. (2008) and de Vente et al. (2013).

715 **7. Acknowledgments**

716 We thank David Cambron and Michele Goodfellow for their help in col-
717 lecting data for this study. This study was based on work supported by a
718 grant from the Florida Fish and Wildlife Conservation Commission and the
719 U.S. Fish and Wildlife Service (State Wildlife Grant 13058). The Geological
720 Society of America, the Gulf Coast Association of Geological Societies, and
721 the University of West Florida Scholarly and Creative Activities Committee
722 provided additional funding. The authors thank Dr. Jim Pizzuto and an
723 anonymous reviewer for their thoughtful critique of this paper. The paper
724 was greatly improved by their comments.

725 **References**

- 726 Allmendinger, N.E., Pizzuto, J.E., Potter, N., Johnson, T.E., Hession, W.C.,
727 2005. The influence of riparian vegetation on stream width, eastern Penn-
728 sylvania, USA. *Geological Society of America Bulletin* 117, 229–243.
729 doi:10.1130/B25447.1.
- 730 Arcement, G.J., Schneider, V.R., 1989. Guide for selecting Manning's rough-
731 ness coefficients for natural channels and flood plains. U.S. Geological Sur-
732 vey Water-Supply Paper 2339, U.S. Government Printing Office, Wash-
733 ton, DC .
- 734 Bandyopadhyay, S., Ghosh, K., De, S.K., 2014. A proposed method of
735 bank erosion vulnerability zonation and its application on the River Haora,
736 Tripura, India. *Geomorphology* 224, 111–121. doi:10.1016/j.geomorph.
737 2014.07.018.
- 738 Bangen, S.G., Wheaton, J.M., Bouwes, N., Bouwes, B., Jordan, C., 2014.
739 A methodological intercomparison of topographic survey techniques for
740 characterizing wadeable streams and rivers. *Geomorphology* 206, 343–361.
741 doi:10.1016/j.geomorph.2013.10.010.
- 742 Bartley, R., Keen, R.J., Hawdon, A.A., Hairsine, P.B., Fisher, M.G., Kinsey-
743 Henderson, A.E., 2008. Bank erosion and channel width change in a trop-
744 ical catchment. *Earth Surface Processes and Landforms* 33, 2174–2200.
745 doi:10.1002/esp.1678.
- 746 Bieger, K., Rathjens, H., Allen, P.M., Arnold, J.G., 2015. Development
747 and evaluation of bankfull hydraulic geometry relationships for the phys-

- 748 iographic regions of the United States. *Journal of the American Water*
749 *Resources Association* 51, 842–858. doi:10.1111/jawr.12282.
- 750 Blanckaert, K., de Vriend, H.J., 2003. Nonlinear modeling of mean flow
751 redistribution in curved open channels. *Water Resources Research* 39,
752 1375. doi:10.1029/2003WR002068.
- 753 Blanckaert, K., de Vriend, H.J., 2010. Meander dynamics: A nonlinear
754 model without curvature restrictions for flow in open-channel bends. *Jour-*
755 *nal of Geophysical Research: Earth Surface* 115, F04011. doi:10.1029/
756 2009JF001301.
- 757 Bull, L.J., 1997. Magnitude and variation in the contribution of bank ero-
758 sion to the suspended sediment load of the River Severn, UK. *Earth*
759 *Surface Processes and Landforms* 22, 1109–1123. doi:10.1002/(SICI)
760 1096-9837(199712)22:12<1109::AID-ESP810>3.0.CO;2-0.
- 761 Camporeale, C., Perona, P., Porporato, A., Ridolfi, L., 2007. Hierarchy
762 of models for meandering rivers and related morphodynamic processes.
763 *Reviews of Geophysics* 45, 5–28. doi:10.1029/2005RG000185.
- 764 Camporeale, C., Ridolfi, L., 2010. Interplay among river meandering, dis-
765 charge stochasticity and riparian vegetation. *Journal of Hydrology* 382,
766 138–144. doi:10.1016/j.jhydrol.2009.12.024.
- 767 Couper, P.R., 2003. Effects of siltclay content on the susceptibility of river
768 banks to subaerial erosion. *Geomorphology* 56, 95–108. doi:10.1016/
769 S0169-555X(03)00048-5.

- 770 Crosato, A., 2009. Physical explanations of variations in river meander migra-
771 tion rates from model comparison. *Earth Surface Processes and Landforms*
772 34, 2078–2086. doi:10.1002/esp.1898.
- 773 Daly, E.R., Miller, R.B., Fox, G.A., 2015. Modeling streambank erosion
774 and failure along protected and unprotected composite streambanks. *Ad-
775 vances in Water Resources* 81, 114–127. doi:10.1016/j.advwatres.2015.
776 01.004.
- 777 Dietrich, W., Bellugi, D., Sklar, L., Stock, J., Heimsath, A., Roering, J.,
778 2003. Geomorphic transport laws for predicting landscape form and dy-
779 namics. In: Wilcock, P., Iverson, R. (Eds.), *Prediction in Geomorphology*.
780 American Geophysical Union, Washington, DC, pp. 103–132.
- 781 Dietrich, W., Smith, J., Dunne, T., 1979. Flow and sediment transport in a
782 sand bedded meander. *The Journal of Geology* 87, 305–315.
- 783 Dietrich, W.E., Smith, J.D., 1983. Influence of the point bar on flow through
784 curved channels. *Water Resources Research* 19, 1173–1192. doi:10.1029/
785 WR019i005p01173.
- 786 Eke, E., Parker, G., Shimizu, Y., 2014. Numerical modeling of erosional
787 and depositional bank processes in migrating river bends with self-formed
788 width: Morphodynamics of bar push and bank pull. *Journal of Geophysical
789 Research: Earth Surface* 119, 1455–1483. doi:10.1002/2013JF003020.
- 790 Faustini, J.M., Kaufmann, P.R., Herlihy, A.T., 2009. Downstream variation
791 in bankfull width of wadeable streams across the conterminous United

- 792 States. Geomorphology 108, 292–311. doi:10.1016/j.geomorph.2009.
793 02.005.
- 794 Ferguson, R., 2010. Time to abandon the Manning equation? Earth Surface
795 Processes and Landforms 35, 1873–1876. doi:10.1002/esp.2091.
- 796 Florsheim, J.L., Mount, J.F., Chin, A., 2008. Bank erosion as a desirable
797 attribute of rivers. BioScience 58, 519–528. doi:10.1641/B580608.
- 798 Gregory, K., 2006. The human role in changing river channels. Geomorphol-
799 ogy 79, 172–191. doi:10.1016/j.geomorph.2006.06.018.
- 800 Güneralp, İ., Filippi, A., Hales, B., 2013. River-flow boundary delineation
801 from digital aerial photography and ancillary images using Support Vector
802 Machines. GIScience & Remote Sensing 50, 1–25. doi:10.1080/15481603.
803 2013.778560.
- 804 Güneralp, İ., Filippi, A.M., Randall, J., 2014. Estimation of floodplain
805 aboveground biomass using multispectral remote sensing and nonpara-
806 metric modeling. International Journal of Applied Earth Observation and
807 Geoinformation 33, 119–126. doi:10.1016/j.jag.2014.05.004.
- 808 Güneralp, İ., Rhoads, B.L., 2007. Continuous characterization of the plan-
809 form geometry and curvature of meandering rivers. Geographical Analysis
810 40, 1–25. doi:10.1111/j.0016-7363.2007.00711.x.
- 811 Güneralp, İ., Rhoads, B.L., 2009. Empirical analysis of the planform
812 curvature-migration relation of meandering rivers. Water Resources Re-
813 search 45, W09424. doi:10.1029/2008WR007533.

- 814 Güneralp, İ., Rhoads, B.L., 2010. Spatial autoregressive structure of me-
815 ander evolution revisited. *Geomorphology* 120, 91–106. doi:10.1016/j.
816 geomorph.2010.02.010.
- 817 Güneralp, İ., Rhoads, B.L., 2011. Influence of floodplain erosional hetero-
818 geneity on planform complexity of meandering rivers. *Geophysical Re-
819 search Letters* 38, 2–7. doi:10.1029/2011GL048134.
- 820 Harmel, R., Haan, C., Dutnall, R., 1999. Evaluation of Rosgen's stream-
821 bank erosion potential assessment in Northeast Oklahoma. *Journal of
822 the American Water Resources Association* 35, 113–121. doi:10.1111/j.
823 1752-1688.1999.tb05456.x.
- 824 Hooke, R., 1975. Distribution of sediment transport and shear stress in a
825 meander bend. *The Journal of Geology* 83, 543–565.
- 826 Hubble, T.C.T., Docker, B.B., Rutherford, I.D., 2010. The role of riparian
827 trees in maintaining riverbank stability: A review of Australian experi-
828 ence and practice. *Ecological Engineering* 36, 292–304. doi:10.1016/j.
829 ecoleng.2009.04.006.
- 830 Hupp, C.R., Simon, A., 1991. Bank accretion and the development of vege-
831 tated depositional surfaces along modified alluvial channels. *Geomorphol-
832 ogy* 4, 111–124. doi:10.1016/0169-555X(91)90023-4.
- 833 Ikeda, S., Parker, G., Sawai, K., 1981. Bend theory of river meanders. Part
834 1. Linear development. *Journal of Fluid Mechanics* 112, 363–377. doi:10.
835 1017/S0022112081000451.

- 836 Julian, J.P., Torres, R., 2006. Hydraulic erosion of cohesive riverbanks. Ge-
837 omorphology 76, 193–206. doi:10.1016/j.geomorph.2005.11.003.
- 838 Kemp, J., Olley, J., Ellison, T., McMahon, J., 2016. River response to
839 European settlement in the subtropical Brisbane River, Australia. An-
840 thropocene doi:10.1016/j.ancene.2015.11.006.
- 841 Knox, J.C., 2006. Floodplain sedimentation in the Upper Mississippi Valley:
842 Natural versus human accelerated. Geomorphology 79, 286–310. doi:10.
843 1016/j.geomorph.2006.06.031.
- 844 Konsoer, K.M., Rhoads, B.L., Langendoen, E.J., Best, J.L., Ursic, M.E.,
845 Abad, J.D., Garcia, M.H., 2016. Spatial variability in bank resistance to
846 erosion on a large meandering, mixed bedrock-alluvial river. Geomorphol-
847 ogy 252, 80–97. doi:10.1016/j.geomorph.2015.08.002.
- 848 Kronvang, B., Andersen, H.E., Larsen, S.E., Audet, J., 2013. Importance
849 of bank erosion for sediment input, storage and export at the catch-
850 ment scale. Journal of Soils and Sediments 13, 230–241. doi:10.1007/
851 s11368-012-0597-7.
- 852 Kwan, H., Swanson, S., 2014. Prediction of Annual Streambank Erosion
853 for Sequoia National Forest, California. Journal of the American Water
854 Resources Association 50, 1439–1447. doi:10.1111/jawr.12200.
- 855 Lawler, D.M., 1993. The measurement of river bank erosion and lateral
856 channel change: A review. Earth Surface Processes and Landforms 18,
857 777–821. doi:10.1002/esp.3290180905.

- 858 Lawler, D.M., Thorne, C.R., Hooke, J.M., 1997. Bank erosion and instability.
859 In: Thorne, C.R., Hey, R.D., Newson, M.D. (Eds.), Applied Fluvial Ge-
860 omorphology for River Engineering and Management. Wiley, Chichester,
861 pp. 137–172.
- 862 Leopold, L.B., Wolman, M.G., 1960. River meanders. Geological Society
863 of America Bulletin 71, 769–793. doi:10.1130/0016-7606(1960)71[769:
864 RM] 2.0.CO;2.
- 865 Lyons, N.J., Starek, M.J., Wegmann, K.W., Mitasova, H., 2015. Bank erosion
866 of legacy sediment at the transition from vertical to lateral stream incision.
867 Earth Surface Processes and Landforms 40, 1764–1778. doi:10.1002/esp.
868 3753.
- 869 Matsubara, Y., Howard, A.D., 2014. Modeling planform evolution of a mud-
870 dominated meandering river: Quinn River, Nevada, USA. Earth Surface
871 Processes and Landforms 39, 1365–1377. doi:10.1002/esp.3588.
- 872 McMillan, M., 2016. Evaluating and developing streambank erosion models
873 in the Gulf of Mexico Coastal Plain. Ph.D. thesis. The University of West
874 Florida.
- 875 Merritts, D.J., Walter, R.C., Rahnis, M., Hartranft, J., Cox, S., Gellis, A.,
876 Potter, N., Hilgartner, W., Langland, M., Manion, L., Lippincott, C.,
877 Siddiqui, S., Rehman, Z., Scheid, C., Kratz, L., Shilling, A., Jenschke,
878 M., Datin, K., Cranmer, E., Reed, A., Matuszewski, D., Voli, M., Ohlson,
879 E., Neugebauer, A., Ahamed, A., Neal, C., Winter, A., Becker, S., 2011.
880 Anthropocene streams and base-level controls from historic dams in the

- 881 unglaciated mid-Atlantic region, USA. Philosophical Transactions of the
882 Royal Society A: Mathematical, Physical, and Engineering Sciences 369,
883 976–1009. doi:10.1098/rsta.2010.0335.
- 884 Metcalf, C.K., Wilkerson, S.D., Harman, W.A., 2009. Bankfull regional
885 curves for North and Northwest Florida streams. Journal of the American
886 Water Resources Association 45, 1260–1272. doi:10.1111/j.1752-1688.
887 2009.00364.x.
- 888 Micheli, E.R., Kirchner, J.W., 2002. Effects of wet meadow riparian vegeta-
889 tion on streambank erosion. 2. Measurements of vegetated bank strength
890 and consequences for failure mechanics. Earth Surface Processes and Land-
891 forms 27, 687–697. doi:10.1002/esp.340.
- 892 Micheli, E.R., Kirchner, J.W., Larsen, E.W., 2004. Quantifying the effect of
893 riparian forest versus agricultural vegetation on river meander migration
894 rates, central Sacramento River, California, USA. River Research and
895 Applications 20, 537–548. doi:10.1002/rra.756.
- 896 Mitchell, K.E., Lohmann, D., Houser, P.R., Wood, E.F., Schaake, J.C.,
897 Robock, A., Cosgrove, B.a., Sheffield, J., Duan, Q., Luo, L., Higgins,
898 R.W., Pinker, R.T., Tarpley, J.D., Lettenmaier, D.P., Marshall, C.H.,
899 Entin, J.K., Pan, M., Shi, W., Koren, V., Meng, J., Ramsay, B.H., Bailey,
900 A.a., 2004. The multi-institution North American Land Data Assimilation
901 System (NLDAS): Utilizing multiple GCIP products and partners in a con-
902 tinental distributed hydrological modeling system. Journal of Geophysical
903 Research 109, D07S90. doi:10.1029/2003JD003823.

- 904 Mosselman, E., 2014. Five common mistakes in fluvial morphodynamic mod-
905 elling. *Advances in Water Resources* 16, 6329. doi:10.1016/j.advwatres.
906 2015.07.025.
- 907 Odgaard, A.J., 1987. Streambank erosion along two rivers in Iowa. *Water*
908 *Resources Research* 23, 1125–1236. doi:10.1029/WR023i007p01225.
- 909 Odgaard, A.J., 1989. River-meander model. II: Applications. *Journal*
910 *of Hydraulic Engineering* 115, 1451–1464. doi:10.1061/(ASCE)
911 0733-9429(1989)115:11(1451).
- 912 Osman, A.M., Thorne, C.R., 1988. Riverbank Stability Analysis. I: The-
913 ory. *Journal of Hydraulic Engineering* 114, 134–150. doi:10.1061/(ASCE)
914 0733-9429(1988)114:2(134).
- 915 Ottevanger, W., Blanckaert, K., Uijttewaal, W.S.J., 2012. Processes govern-
916 ing the flow redistribution in sharp river bends. *Geomorphology* 163-164,
917 45–55. doi:10.1016/j.geomorph.2011.04.049.
- 918 Ottevanger, W., Blanckaert, K., Uijttewaal, W.S.J., de Vriend, H.J., 2013.
919 Meander dynamics: A reduced-order nonlinear model without curvature
920 restrictions for flow and bed morphology. *Journal of Geophysical Research:*
921 *Earth Surface* 118, 1118–1131. doi:10.1002/jgrf.20080.
- 922 Parker, G., Shimizu, Y., Wilkerson, G.V., Eke, E.C., Abad, J.D., Lauer,
923 J.W., Paola, C., Dietrich, W.E., Voller, V.R., 2011. A new framework for
924 modeling the migration of meandering rivers. *Earth Surface Processes and*
925 *Landforms* 36, 70–86. doi:10.1002/esp.2113.

- 926 Partheniades, E., 1965. Erosion and deposition of cohesive soils. *Journal*
927 of the Hydraulics Division of the American Society of Civil Engineers 91,
928 105–139.
- 929 Pelletier, J.D., 2012. A spatially distributed model for the long-term sus-
930 pended sediment discharge and delivery ratio of drainage basins. *Journal*
931 of Geophysical Research 117, F02028. doi:10.1029/2011JF002129.
- 932 Pelletier, J.D., Brad Murray, A., Pierce, J.L., Bierman, P.R., Breshears,
933 D.D., Crosby, B.T., Ellis, M., Foufoula-Georgiou, E., Heimsath, A.M.,
934 Houser, C., Lancaster, N., Marani, M., Merritts, D.J., Moore, L.J.,
935 Pederson, J.L., Poulos, M.J., Rittenour, T.M., Rowland, J.C., Rug-
936 giero, P., Ward, D.J., Wickert, A.D., Yager, E.M., 2015. Forecasting
937 the response of Earth's surface to future climatic and land use changes:
938 A review of methods and research needs. *Earth's Future* 3, 220–251.
939 doi:10.1002/2014EF000290.
- 940 Perucca, E., Camporeale, C., Ridolfi, L., 2007. Significance of the riparian
941 vegetation dynamics on meandering river morphodynamics. *Water Re-
942 sources Research* 43, W03430. doi:10.1029/2006WR005234.
- 943 Pizzuto, J.E., 1984. Bank erodibility of shallow sandbed streams. *Earth Sur-*
944 *face Processes and Landforms* 9, 113–124. doi:10.1002/esp.3290090203.
- 945 Pizzuto, J.E., Meckelnburg, T.S., 1989. Evaluation of a linear bank ero-
946 sion equation. *Water Resources Research* 25, 1005–1013. doi:10.1029/
947 WR025i005p01005.

- 948 Pizzuto, J.E., O'Neal, M., 2009. Increased mid-twentieth century riverbank
949 erosion rates related to the demise of mill dams, South River, Virginia.
950 Geology 37, 19–22. doi:10.1130/G25207A.1.
- 951 Pizzuto, J.E., O'Neal, M., Stotts, S., 2010. On the retreat of forested, cohe-
952 sive riverbanks. Geomorphology 116, 341–352. doi:10.1016/j.geomorph.
953 2009.11.008.
- 954 Pollen, N., 2007. Temporal and spatial variability in root reinforcement of
955 streambanks: Accounting for soil shear strength and moisture. Catena 69,
956 197–205. doi:10.1016/j.catena.2006.05.004.
- 957 Pollen, N., Simon, A., 2005. Estimating the mechanical effects of riparian
958 vegetation on stream bank stability using a fiber bundle model. Water
959 Resources Research 41, W07025. doi:10.1029/2004WR003801.
- 960 Rosgen, D.L., 1994. A classification of natural rivers. Catena 22, 169–199.
961 doi:10.1016/0341-8162(94)90001-9.
- 962 Rosgen, D.L., 2001. A practical method of computing streambank erosion
963 rate. In: Proceedings of the Seventh Federal Interagency Sedimentation
964 Conference, US Inter-agency Committee on Water Resources, Subcommit-
965 tee on Sedimentation. pp. 9–18.
- 966 Rosgen, D.L., 2009. Watershed Assessment of River Stability and Sediment
967 Supply. 2 ed., Wildland Hydrology.
- 968 Rossi, M.W., Whipple, K.X., Vivoni, E.R., 2016. Precipitation and evapo-
969 transpiration controls on daily runoff variability in the contiguous United

- 970 States and Puerto Rico. *Journal of Geophysical Research: Earth Surface*
971 121, 128–145. doi:10.1002/2015JF003446.
- 972 Sass, C.K., Keane, T.D., 2012. Application of Rosgen's BANCS model for
973 NE Kansas and the development of predictive streambank erosion curves.
974 *Journal of the American Water Resources Association* 48, 774–787. doi:10.
975 1111/j.1752-1688.2012.00644.x.
- 976 Sefick, S.A., Kalin, L., Kosnicki, E., Schneid, B.P., Jarrell, M.S., Anderson,
977 C.J., Paller, M.H., Fominella, J.W., 2015. Empirical estimation of stream
978 discharge using channel geometry in low-gradient, sand-bed streams of the
979 Southeastern Plains. *Journal of the American Water Resources Association*
980 51, 1060–1071. doi:10.1111/jawr.12278.
- 981 Sekely, A., Mulla, D., Bauer, D., 2002. Streambank slumping and its contri-
982 bution to the phosphorus and suspended sediment loads of the Blue Earth
983 River, Minnesota. *Journal of Soil and Water Conservation* 57, 243–250.
- 984 Sexton, J.O., Song, X.P., Feng, M., Noojipady, P., Anand, A., Huang, C.,
985 Kim, D.H., Collins, K.M., Channan, S., Dimiceli, C., Townshend, J.R.,
986 2013. Global, 30-m resolution continuous fields of tree cover: Landsat-
987 based rescaling of MODIS Vegetation Continuous Fields with lidar-based
988 estimates of error. *International Journal of Digital Earth* 6, 427–448.
989 doi:10.1080/17538947.2013.786146.
- 990 Simon, A., Curini, A., Darby, S., Langendoen, E., 2000. Bank and near-bank
991 processes in an incised channel. *Geomorphology* 35, 193–217. doi:10.1016/
992 S0169-555X(00)00036-2.

- 993 Simon, A., Doyle, M., 2007. Critical evaluation of how the Rosgen classifi-
994 cation and associated “Natural Channel Design” methods fail to integrate
995 and quantify fluvial processes and channel response. *Journal of the Amer-*
996 *ican Water Resources Association* 43, 1117–1131.
- 997 Stott, T., 1997. A comparison of stream bank erosion processes on forested
998 and moorland streams in the Balquhidder Catchments, central Scotland.
999 *Earth Surface Processes and Landforms* 22, 383–399. doi:10.1002/(SICI)
1000 1096-9837(199704)22:4<383::AID-ESP695>3.0.CO;2-4.
- 1001 Thomas, R.E., Pollen-Bankhead, N., 2010. Modeling root-reinforcement with
1002 a fiber-bundle model and Monte Carlo simulation. *Ecological Engineering*
1003 36, 47–61. doi:10.1016/j.ecoleng.2009.09.008.
- 1004 Thorne, C., 1982. Processes and mechanisms of river bank erosion. In: Hey,
1005 R., Bathurst, J., Thorne, C. (Eds.), *Gravel-Bed Rivers: Processes, Tools,*
1006 *Environments*. Wiley, Chichester, pp. 227–271.
- 1007 Thorne, S.D., Furbish, D.J., 1995. Influences of coarse bank roughness on
1008 flow within a sharply curved river bend. *Geomorphology* 12, 241–257.
1009 doi:10.1016/0169-555X(95)00007-R.
- 1010 Tiwari, H., Das, P., Bharti, A.K., 2012. MATLAB programming solution for
1011 critical and normal depth in trapezoidal channels. *International Journal*
1012 *of Engineering Research and Technology* 1, 1–3.
- 1013 U.S. Environmental Protection Agency, 2000. National Water Quality In-
1014 ventory .

- 1015 Van Eps, M.A., Formica, S.J., Morris, T.L., Beck, J.M., Cotter, A.S., 2004.
1016 Using a bank erosion hazard index (BEHI) to estimate annual sediment
1017 loads from streambank erosion in the West Fork White River watershed.
1018 In: Self-Sustaining Solutions for Streams, Wetlands, and Watersheds,
1019 12-15, September 2004, American Society of Agricultural and Biologi-
1020 cal Engineers. American Society of Agricultural and Biological Engineers.
1021 doi:10.13031/2013.17386.
- 1022 Vatankhah, A.R., 2013. Explicit solutions for critical and normal depths in
1023 trapezoidal and parabolic open channels. Ain Shams Engineering Journal
1024 4, 17–23. doi:10.1016/j.asej.2012.05.002.
- 1025 de Vente, J., Poesen, J., Verstraeten, G., Govers, G., Vanmaercke, M., Van
1026 Rompaey, A., Arabkhedri, M., Boix-Fayos, C., 2013. Predicting soil erosion
1027 and sediment yield at regional scales: Where do we stand? Earth-Science
1028 Reviews 127, 16–29. doi:10.1016/j.earscirev.2013.08.014.
- 1029 Walter, R.C., Merritts, D.J., 2008. Natural streams and the legacy of water-
1030 powered mills. Science 319, 299–304. doi:10.1126/science.1151716.
- 1031 Wilkinson, S.N., Dougall, C., Kinsey-Henderson, A.E., Searle, R.D., Ellis,
1032 R.J., Bartley, R., 2014. Development of a time-stepping sediment budget
1033 model for assessing land use impacts in large river basins. Science of the
1034 Total Environment 468-469, 1210–1224. doi:10.1016/j.scitotenv.2013.
1035 07.049.
- 1036 Wilkinson, S.N., Prosser, I.P., Rustomji, P., Read, A.M., 2009. Modelling and
1037 testing spatially distributed sediment budgets to relate erosion processes

- 1038 to sediment yields. *Environmental Modelling and Software* 24, 489–501.
1039 doi:10.1016/j.envsoft.2008.09.006.
- 1040 Wynn, T.M., Mostaghimi, S., 2006. The effects of vegetation and soil type on
1041 streambank erosion, southwestern Virginia, USA. *Journal of the American
1042 Water Resources Association* 42, 69–82. doi:DOI:10.1111/j.1752-1688.
1043 2006.tb03824.x.
- 1044 Xia, Y., Mitchell, K., Ek, M., Cosgrove, B., Sheffield, J., Luo, L., Alonge, C.,
1045 Wei, H., Meng, J., Livneh, B., Duan, Q., Lohmann, D., 2012. Continental-
1046 scale water and energy flux analysis and validation for North American
1047 Land Data Assimilation System project phase 2 (NLDAS-2): 2. Validation
1048 of model-simulated streamflow. *Journal of Geophysical Research: Atmo-
1049 spheres* 117, D03110. doi:10.1029/2011JD016051.
- 1050 Xiao, X., White, E.P., Hooten, M.B., Durham, S.L., 2011. On the use of
1051 log-transformation vs. nonlinear regression for analyzing biological power
1052 laws. *Ecology* 92, 1887–1894. doi:10.1890/11-0538.1.
- 1053 Zeng, X., 2001. Global vegetation root distribution for land modeling.
1054 *Journal of Hydrometeorology* 2, 525–530. doi:10.1175/1525-7541(2001)
1055 002<0525:GVRDFL>2.0.CO;2.